Simple analytical–statistical models (ASMs) for mean annual permafrost table temperature and active-layer thickness estimates

Tomáš Uxa[1,2], Filip Hrbáček[2], and Michaela Kňažková[2]

[1]Institute of Geophysics, Czech Academy of Sciences, Prague, Czech Republic
[2]Polar-Geo-Lab, Department of Geography, Faculty of Science, Masaryk University, Brno, Czech Republic

Correspondence: Tomáš Uxa (uxa@ig.cas.cz)

Abstract. A variety of numerical, analytical and statistical number of models have been developed for estimating the mean annual permafrost table temperature (MAPT) and active-layer thickness (ALT). These tools typically require at least a few ground physical properties , such as thermal conductivity, heat capacity, water content or bulk density, as as their input parameters in addition to temperature variables, which are, however, unavailable or unrepresentative at most sites. Ground air or ground temperatures. However, ground physical properties are therefore commonly frequently unavailable or unrepresentative and therefore need to be estimated, which may yield model outputsof unknown validityintroduces uncertainties into model outputs. Hence, we devised two simple analytical–statistical models (ASMs) for estimating MAPT and ALT, which are driven solely by pairwise combinations of thawing and freezing indices in from two depth levels within the active layer;, while no ground physical properties are required. ASMs reproduced MAPT and ALT well in most numerical validations, which corroborated their theoretical assumptions under idealized scenarios. Under field conditions of Antarctica and Alaska, the mean ASMs deviations in MAPT and ALT were less than 0.03in the Earth's major permafrost regions with the total mean errors of less than 0.05 °C and 58 %, respectively, which . This is similar or better than other analytical or statistical models. This , which suggests that ASMs can be useful tools for estimating MAPT and ALT under a wide range of climates and ground physical environmental conditions.

1 Introduction

Of ∼11 % of the Earth's exposed land surface underlain by permafrost (Obu, 2021), most seasonally thaws from the ground surface to a depth of up to several meters and then completely refreezes(active layer), which is mainly controlled by climate conditions and ground physical properties (Bonnaventure and Lamoureux, 2013). The This superficial active layer greatly influences the energy and mass transfer between the underlying permafrost, ground surface and the atmosphere, and is therefore critical for the dynamics of hydrologichydrological, geomorphic, pedogenic, biologic andbiogeochemic biological and/or biogeochemical processes including greenhouse gas fluxes, as well as for human infrastructure in permafrost regions (e.g., Grosse et al., 2016; Walvoord and Kurylyk, 2016; Hjort et al., 2022). As climate is a first-order control on ground temperatures and thaw depth (Wang et al., 2019; Smith et al., 2022), the thermal state of permafrost and the thickness of the active layer have attracted a huge interest over recent decades because they are important measures indicators of how the climate system is evolving (Li et al., 2022; Hrbáček et al., 2023b). ~~Besides that, climate changes have~~ Climate change has provoked permafrost warming and active-layer thickening at a global scale ~~(Biskaborn et al., 2019; Noetzli et al., 2024)~~(Noetzli et al., 2024; Smith et al., 2024), which can have severe consequences on landscape and ecosystem stability as well as infrastructure integrity. Carbon release due to permafrost degradation is likely to trigger feedback mechanisms with impacts on the Earth's climate system (Lawrence et al., 2015; Schuur et al., 2022). The permafrost and active-layer monitoring is therefore of utmost scientific and societal importance (Brown et al., 2000; Biskaborn et al., 2015).

The thermal state of permafrost and the thickness of the active layer have ~~commonly~~ been investigated by semi-continuous temperature measurements using data loggers with temperature sensors distributed in vertical arrays across the active layer and near-surface permafrost (e.g., Biskaborn et al., 2015; Noetzli et al., 2021), by periodic or semi-continuous geophysical measurements using electric, electromagnetic or seismic methods (e.g., Hauck, 2002; Farzamian et al., 2020), or by periodic thaw-depth measurements using physical probing with rigid rods or thaw-tube readings (e.g., Burn, 1998; Bonnaventure and Lamoureux, 2013). Of these methods, temperature measurements using data loggers are the most convenient in terms of accuracy, temporal resolution and/or logistics, which is well suitable for ~~frequently~~ remote and poorly accessible permafrost regions that have limited or no technical infrastructure ~~(Brown et al., 2000; Biskaborn et al., 2015). At many places, however, temperatures are only measured~~ (Biskaborn et al., 2015; Streletskiy et al., 2022). However, ground temperatures are frequently measured only in the active layer, and therefore the permafrost temperatures and the active-layer thickness ~~must therefore~~ need to be estimated in these situations. This has been done using either statistical methods or numerical and analytical models of various complexity ~~(e.g., Riseborough et al., 2008; Bonnaventure and Lamoureux, 2013; Aalto et al., 2018)~~ (e.g., Riseborough, 2008; Riseborough et al., 2008; Bonnaventure and Lamoureux, 2013; Aalto et al., 2018).

Of these solutions, analytical models in particular have become ~~widely~~ popular for estimating the mean annual temperature at the ~~base of the active layer or the~~ top of permafrost (hereafter referred to as the mean annual permafrost table temperature, MAPT) (Garagulya, 1990; Romanovsky and Osterkamp, 1995; Smith and Riseborough, 1996) and the active-layer thickness (ALT) (Neumann, c. 1860; Stefan, 1891; Kudryavtsev et al., 1977) because of their simplicity, small number of input parameters, computational efficiency and yet sufficient accuracy, which is ~~highly~~ advantageous for diverse permafrost regions and environmental settings (e.g., Anisimov et al., 1997; Nelson et al., 1997; Zhao et al., 2017; Obu et al., 2019, 2020). ~~However, these tools~~ These tools typically require at least a few ground physical properties, such as thermal conductivity, heat capacity, water content or bulk density, as their input parameters in addition to ~~temperature variables, which are seldom available at most sites. Ground~~ air or ground temperatures. However, ground physical properties are ~~therefore commonly~~ frequently unavailable or unrepresentative and therefore need to be estimated, which ~~may yield model outputsof unknown validity~~introduces uncertainties into model outputs. But even ~~in-situ measurements~~ *in situ* observations of ground physical properties may not guarantee accurate model outputs either, as ~~they are usually taken~~ these properties are usually measured annually or less frequently and are then ~~typically~~ treated as constants in models, regardless of their temporal variability, which can be considerable (e.g., Gao et al., 2020; Hrbáček et al., 2023a; Li et al., 2023; Kňažková and Hrbáček, 2024; Wenhao et al., 2024).

Here, we devise two novel analytical–statistical models (ASMs) for MAPT and ALT, which are driven solely by thawing and freezing indices ~~at two distinct depths in~~ from two depth levels within the active layer~~to address the general lack and /or non-representativeness of ground physical data for permafrost models. We test these solutions against numerical model simulations for idealized scenarios as well as against field observations from distinct permafrost environments of Antarctica and Alaska~~. ASMs are primarily intended to be used for MAPT or ALT estimates where ground temperature measurements are too shallow and MAPT or ALT therefore cannot be determined directly, while no information on ground physical properties exists. We evaluate ASMs against *in situ* ground temperature measurements from the Earth's major permafrost regions, and we discuss their performance, advantages and limitations.

2 Model ~~derivations~~derivation

2.1 Mean annual permafrost table temperature

~~Besides other solution (Garagulya, 1990),~~ MAPT [°C] can be calculated ~~by~~ using the TTOP model (Romanovsky and Osterkamp, 1995; Smith and Riseborough, 1996), which assumes that the ratio of thawed and frozen thermal conductivity and the effects of latent heat produce the difference between MAPT and the mean annual ground surface temperature (thermal offset). The TTOP formula for permafrost conditions (MAPT $\leq 0\,°\mathrm{C}$) is as follows (Romanovsky and Osterkamp, 1995; Smith and Riseborough, 1996)

$$\mathrm{MAPT} = \frac{\frac{k_t}{k_f} I_{ts} - I_{fs}}{P}, \tag{1}$$

where k_t [W m^{-1} K^{-1}] and k_f [W m^{-1} K^{-1}] is the thawed and frozen thermal conductivity, respectively, that defines the thermal conductivity ratio, I_{ts} [°C d] and I_{fs} [°C d] is the ground surface thawing and freezing index, respectively (both ~~expressed degree-days and~~ assumed in absolute values), and P [365 d] is the length of one year.

~~Besides surface temperatures~~However, Eq. (1) ~~is valid for temperatures~~ can work with thawing and freezing index measured at any depth ~~in~~ within the active layer ~~, which~~ (Riseborough, 2004). This is highly convenient because ground surface ~~temperature is~~ temperatures are difficult to measure due to ~~surface~~ radiative and convective energy fluxes and ~~due to~~ problematic fixing of temperature sensors exactly at the ground surface ~~level (Riseborough, 2003). Hence, MAPT based on~~ (Riseborough, 2003). Using ground temperatures measured at two ~~distinct depths in~~ depth levels within the active layer z_1 and z_2 ($z_1 < z_2 <$ ALT)~~can~~, MAPT can therefore be expressed as ~~follows~~

$$\mathrm{MAPT} = \frac{\frac{k_t}{k_f} I_{tz_1} - I_{fz_1}}{P}, \tag{2}$$

$$\mathrm{MAPT} = \frac{\frac{k_t}{k_f} I_{tz_2} - I_{fz_2}}{P}, \tag{3}$$

where I_{tz_1} [°C d] and I_{fz_1} [°C d] is the thawing and freezing index ~~, respectively,~~ at the depth z_1, and I_{tz_2} [°C d] and I_{fz_2} [°C d] is the thawing and freezing index ~~, respectively,~~ at the depth z_2. This implies that Eq. (2) and (3) are equivalent:

$$\frac{\frac{k_t}{k_f} I_{tz_1} - I_{fz_1}}{P} = \frac{\frac{k_t}{k_f} I_{tz_2} - I_{fz_2}}{P}. \tag{4}$$

Solving Eq. (4) for the thermal conductivity ratio yields

$$\frac{k_t}{k_f} = \frac{I_{fz_1} - I_{fz_2}}{I_{tz_1} - I_{tz_2}}. \tag{5}$$

Equation (5) can be ~~then~~ substituted for the thermal conductivity ratio in Eq. (2) and (3) as follows

$$\mathrm{MAPT} = \frac{\frac{I_{fz_1} - I_{fz_2}}{I_{tz_1} - I_{tz_2}} I_{tz_1} - I_{fz_1}}{P}, \tag{6}$$

$$\mathrm{MAPT} = \frac{\frac{I_{fz_1} - I_{fz_2}}{I_{tz_1} - I_{tz_2}} I_{tz_2} - I_{fz_2}}{P}. \tag{7}$$

~~Subsequently,~~ Simplifying Eq. (6) and (7) ~~both simplify to~~ then produces the same formula for MAPT:

$$\mathrm{MAPT} = \frac{\frac{I_{fz_1} I_{tz_2} - I_{fz_2} I_{tz_1}}{I_{tz_1} - I_{tz_2}}}{P}. \tag{8}$$

Substantially, Eq. (8) implies that MAPT can be simply estimated using thawing and freezing indices ~~at two distinct depths in~~ from two depth levels within the active layer alone, that is, without ~~the knowledge of the~~ knowing the thermal conductivity ratio.

~~While~~ Since Eq. (8) was derived from Eq. (1), it has a physical basis (cf. Romanovsky and Osterkamp, 1995). However, it can be shown that it is in principle a linear extrapolation of the freezing index to the depth, where the thawing index becomes zero, ~~with the slope defined by the thermal conductivity ratio, and its division~~ and dividing it by the length of one year. Using the same notation as before, this can be expressed as ~~follows~~

$$\frac{I_{fz_1} - I_{f_{\mathrm{ALT}}}}{I_{tz_1} - I_{t_{\mathrm{ALT}}}} = \frac{I_{fz_1} - I_{fz_2}}{I_{tz_1} - I_{tz_2}}, \tag{9}$$

$$\frac{I_{fz_2} - I_{f_{\mathrm{ALT}}}}{I_{tz_2} - I_{t_{\mathrm{ALT}}}} = \frac{I_{fz_1} - I_{fz_2}}{I_{tz_1} - I_{tz_2}}, \tag{10}$$

where $I_{t_{\mathrm{ALT}}}$ [°C d] and $I_{f_{\mathrm{ALT}}}$ [°C d] represents the thawing and freezing index at the base of the active layer. Note that the slope of the relationship is determined by the thermal conductivity ratio. Solving Eq. (9) and (10) for $I_{f_{\mathrm{ALT}}}$ gives

$$-I_{f_{\mathrm{ALT}}} = \frac{I_{fz_1} - I_{fz_2}}{I_{tz_1} - I_{tz_2}} (I_{tz_1} - I_{t_{\mathrm{ALT}}}) - I_{fz_1}, \tag{11}$$

$$-I_{f_{\mathrm{ALT}}} = \frac{I_{fz_1} - I_{fz_2}}{I_{tz_1} - I_{tz_2}} (I_{tz_2} - I_{t_{\mathrm{ALT}}}) - I_{fz_2}. \tag{12}$$

Since the thawing index at the base of the active layer is zero, Eq. (11) and (12) become equivalent to Eq. (6) and (7), respectively, when divided by the length of one year, and both simplify to Eq. (8). This documents that Eq. (8) ~~for MAPT is~~ can be derived in two alternative manners consisting of analytical and statistical ~~at the same time because it integrates both approaches~~procedures.

2.2 Active-layer thickness

~~Besides other solutions (Neumann, c. 1860; Kudryavtsev et al., 1977),~~ ALT [m] can be calculated ~~by~~ using the Stefan (1891) model, which builds on the premise that the conductive heat flux above the thaw front equals to the rate at which latent heat is absorbed as the thaw front propagates downwards. Its simplest form is as follows (Lunardini, 1981)

$$\mathrm{ALT} = \sqrt{\frac{2k_t I_{ts}}{L\phi}}, \tag{13}$$

where L [3.34×10^8 J m^{-3}] is the volumetric latent heat of fusion of water and ϕ [–] is the volumetric water content. Note that the thawing index must be multiplied by the scaling factor of 86 400 s d^{-1} ~~in the Stefan model to yield correct outputs~~. As stated previously (Sect. 2.1), ~~the ground surface temperature is~~ ground surface temperatures are difficult to measure (Riseborough, 2003), and therefore the Stefan model has commonly been forced by ~~temperatures recorded~~ ground temperatures collected at some depth ~~in~~ within the active layer. However, this has rarely been accounted for, although it has been shown to substantially affect the model outputs ~~(Hrbáček and Uxa, 2020; Kaplan Pastíriková et al., 2023), and~~ (Hrbáček and Uxa, 2020; Kaplan Pastíriková et al., 2023). Yet, it can be easily implemented as follows (Riseborough, 2003; Hayashi et al., 2007)

$$\mathrm{ALT} = z + \sqrt{\frac{2k_t I_{tz}}{L\phi}}, \tag{14}$$

where z [m] ~~represents the depth where the forcing temperature was measured and~~ is the depth at which the thawing index I_{tz} [°C d] is ~~the thawing index at the depth z. ALT estimated using thawing indices~~ measured. Using ground temperatures measured at two ~~distinct depths in~~ depth levels within the active layer z_1 and z_2 ($z_1 < z_2 < \mathrm{ALT}$)~~can~~, ALT can therefore be expressed as ~~follows~~

$$\mathrm{ALT} = z_1 + \sqrt{\frac{2k_t I_{tz_1}}{L\phi}}, \tag{15}$$

$$\mathrm{ALT} = z_2 + \sqrt{\frac{2k_t I_{tz_2}}{L\phi}}. \tag{16}$$

This implies that Eq. (15) and (16) are equivalent:

$$z_1 + \sqrt{\frac{2k_t I_{tz_1}}{L\phi}} = z_2 + \sqrt{\frac{2k_t I_{tz_2}}{L\phi}}. \tag{17}$$

The vertical distance between z_2 and z_1 can be expressed as

$$z_2 - z_1 = \sqrt{\frac{2k_t I_{tz_1}}{L\phi}} - \sqrt{\frac{2k_t I_{tz_2}}{L\phi}}, \tag{18}$$

which simplifies to

$$z_2 - z_1 = \sqrt{\frac{2k_t}{L\phi}}\left(\sqrt{I_{tz_1}} - \sqrt{I_{tz_2}}\right). \tag{19}$$

Subsequently rearranging Eq. (19) gives

$$\frac{z_2 - z_1}{\sqrt{I_{tz_1}} - \sqrt{I_{tz_2}}} = \sqrt{\frac{2k_t}{L\phi}}, \tag{20}$$

where the right-hand side corresponds to the so-called edaphic term (Nelson and Outcalt, 1987), which has previously been used in numerous studies (Nelson and Outcalt, 1987; Hinkel and Nicholas, 1995; Nelson et al., 1997; Anisimov et al., 2002; Shiklomanov been used to combine the ground physical properties in the Stefan model thawed thermal conductivity and volumetric water content into a single variable as follows in the modified Stefan model:

$$\mathrm{ALT} = E\sqrt{I_{tz}}\sqrt{I_{ts}}, \tag{21}$$

where E [m s$^{-0.5}$ K$^{-0.5}$] [m °C d$^{-0.5}$] denotes the edaphic term given by

$$E = \sqrt{\frac{2k_t}{L\phi}}. \tag{22}$$

Usually, Although Eq. (21) has been referred to as the modified Stefan model and proved to be useful in situations where the ground physical properties were unavailable and/or for spatial modelling of ALT (Nelson and Outcalt, 1987; Hinkel and Nicholas, 1995; Ne . Its major advantage is that it can largely overcome many of the shortcomings of the simplistic Stefan model (is equivalent to Eq. (13), which assumes that the ground physical properties throughout the active layer are constant, the active-layer temperature decreases linearly from the surface to the bottom frozen layer that is at 0 C, and the conductive heat flux is fully consumed by latent heat to thaw the active layer (Kurylyk, 2015). However, the value of the edaphic term has only been derived based on empirical relationships it has frequently been preferred for estimating ALT because the edaphic term can be calibrated based on the relationship between ALT and thawing indexin several thawing seasons and/or at multiple locations (Nelson et al., 1997; Anisimov et al., 2002; Shiklomanov and Nelson, 2002; Peng et al., 2023). This led on the one hand to its high accuracy for the calibration conditions, but on the other hand had limitations in terms of its transferability to other thawing seasons and/or locations. Notwithstanding that , the that is, without knowing the thawed thermal conductivity and volumetric water content (Nelson and Outcalt, 1987; Hinkel and Nicholas, 1995; Nelson et al., 1997; Anisimov et al., 2002; Shiklomanov and Nelson . The edaphic term can be implemented in Eq. (15) and (16) as follows

$$\mathrm{ALT} = z_1 + E\sqrt{I_{tz_1}}, \tag{23}$$

$$\mathrm{ALT} = z_2 + E\sqrt{I_{tz_2}}. \tag{24}$$

Substituting the left-hand side of Eq. (20) for the edaphic term in Eq. (23) and (24) yields

$$\mathrm{ALT} = z_1 + \frac{z_2 - z_1}{\sqrt{I_{tz_1}} - \sqrt{I_{tz_2}}}\sqrt{I_{tz_1}}, \tag{25}$$

$$\mathrm{ALT} = z_2 + \frac{z_2 - z_1}{\sqrt{I_{tz_1}} - \sqrt{I_{tz_2}}}\sqrt{I_{tz_2}}. \tag{26}$$

Simplifying Eq. (25) and (26) then produces the same formula for ALT:

$$\mathrm{ALT} = \frac{z_2\sqrt{I_{tz_1}} - z_1\sqrt{I_{tz_2}}}{\sqrt{I_{tz_1}} - \sqrt{I_{tz_2}}}. \tag{27}$$

Substantially, Eq. (27) implies that ALT can be simply estimated using thawing indices ~~at two distinct depths in~~ from two depth levels within the active layer alone, that is, without ~~the knowledge of the ground physical properties~~ knowing the thawed thermal conductivity and volumetric water content or the edaphic term.

~~While~~ Since Eq. (27) was derived from Eq. (13), it has a physical basis (cf. Lunardini, 1981). However, it can also be shown that it is in principle a linear extrapolation of the depth ~~at which~~ where the square root of the thawing ~~indices~~ index becomes zero (cf. Riseborough, 2003)~~, with the slope defined by the edaphic term. Using the same notation as before, this~~. This can be expressed as ~~follows~~

$$\frac{\mathrm{ALT} - z_1}{\sqrt{I_{tz_1}} - \sqrt{I_{t_{\mathrm{ALT}}}}} = \frac{z_2 - z_1}{\sqrt{I_{tz_1}} - \sqrt{I_{tz_2}}}, \tag{28}$$

$$\frac{\mathrm{ALT} - z_2}{\sqrt{I_{tz_2}} - \sqrt{I_{t_{\mathrm{ALT}}}}} = \frac{z_2 - z_1}{\sqrt{I_{tz_1}} - \sqrt{I_{tz_2}}}. \tag{29}$$

Note that the slope of the relationship is determined by the edaphic term. Solving Eq. (28) and (29) for ALT gives

$$\mathrm{ALT} = z_1 + \frac{z_2 - z_1}{\sqrt{I_{tz_1}} - \sqrt{I_{tz_2}}}\left(\sqrt{I_{tz_1}} - \sqrt{I_{t_{\mathrm{ALT}}}}\right), \tag{30}$$

$$\mathrm{ALT} = z_2 + \frac{z_2 - z_1}{\sqrt{I_{tz_1}} - \sqrt{I_{tz_2}}}\left(\sqrt{I_{tz_2}} - \sqrt{I_{t_{\mathrm{ALT}}}}\right). \tag{31}$$

Since the thawing index at the base of the active layer is zero, Eq. (30) and (31) are equivalent to Eq. (25) and (26), respectively, and both simplify to Eq. (27). As with Eq. (8), this documents that Eq. (27) ~~for ALT is~~ can also be derived in two alternative manners consisting of analytical and statistical ~~at the same time because it integrates both approaches~~procedures.

3 Model ~~validations~~evaluation

~~The validity of~~ ASMs for estimating MAPT and ALT ~~given by Eq. (8) and (27), respectively, was tested in a twofold manner, with ground temperatures simulated by a simple one-dimensional numerical model for idealized scenarios and those from field observations.~~

3.1 ~~Idealized scenarios~~

~~We considered five scenarios with a mean annual air temperature (MAAT) of −12~~were evaluated using *in situ* ground temperature measurements from the Earth's major permafrost regions that differ in climate, permafrost zone, ground surface cover and/or ground physical properties and their distribution within the active layer to enhance the robustness of the model evaluation. Since the accuracy of the observed ALT depends on the distance between the ground temperature sensors (Riseborough, 2003, 2008), we arbitrarily set their maximum spacing at 25 ~~C, −10 C, −8 C, −6 C and −4 C that varied sinusoidally over a year within~~

a range of cm and 40 C. The air temperatures were converted to ground surface temperature series using linear scaling with so-called thawing andfreezing n-factors of 1 and 0.5, respectively (Lunardini, 1978). Ground temperatures were then simulated using a one-dimensional numerical model by solving the transient heat conduction equation with phase changes (Carslaw and Jaeger, 1959):

$$C_{\text{eff}} \frac{\partial T}{\partial t} = \frac{\partial}{\partial z}\left(k \frac{\partial T}{\partial z}\right),$$

where C_{eff} [J m^{-3} K^{-1}] is the apparent volumetric heat capacity, T [°C] is the temperature, t [s] is the time, and k [W m^{-1} K^{-1}] is the thermal conductivity. Ground was set to be fully frozen and thawed at T_f [−0.05 °C] and T_t [0.05 °C], respectively, and linear intermediate in between. Although simplistic, this was chosen to be as close as possible to ASMs, which assume a water—ice transition at 0cm for ALT of <1 C, while ensuring numerical stability. Similar to Sun et al. (2020), the apparent volumetric heat capacity and thermal conductivity accounted for phase changes with latent heat effects as follows

$$C_{\text{eff}} = \begin{cases} C_f & \text{for } T \le T_f \\ C_f + (C_t - C_f)\frac{T-T_f}{T_t-T_f} + \frac{L\phi}{T_t-T_f} & \text{for } T_f < T \le T_t \\ C_t & \text{for } T > T_t \end{cases},$$

$$k = \begin{cases} k_f & \text{for } T \le T_f \\ k_f + (k_t - k_f)\frac{T-T_f}{T_t-T_f} & \text{for } T_f < T \le T_t \\ k_t & \text{for } T > T_t \end{cases},$$

where C_f [J m^{-3} K^{-1}] and C_t [J m^{-3} K^{-1}] is the frozen and thawed volumetric heat capacity, respectively. The values of the frozen thermal conductivity and the frozen volumetric heat capacity were estimated from the thawed ones based on the volumetric water content as follows (**?**)

$$k_f = k_t\left(\frac{k_i}{k_w}\right)^{\phi},$$

$$C_f = C_t - \phi(C_w - C_i),$$

where k_i [2.22 W m^{-1} K^{-1}] is the thermal conductivity of ice, k_w [0.57 W m^{-1} K^{-1}] is the thermal conductivity of water, C_w [4.21×10^6 J m^{-3} is the volumetric heat capacity of water, and C_i [2.05×10^6 J m^{-3} K^{-1}] is the volumetric heat capacity of ice.

One- and two-layer profiles representing mineral soil alone and 20 cm of peat over mineral soil, respectively, that had constant physical properties except for phase changes were considered in these numerical tests (Table 1), as they aimed to demonstrate the viability of ASMs under idealized conditions. Since ASMs assume a homogeneous profile, the two-layer profile was to examine their behaviour when this condition is not met.

Values of ground physical properties used in the numerical model simulations for idealized scenarios. Variable Value UnitPeatDepth 0–0.2 m Thawed thermal conductivity 0.50 W m^{-1} K^{-1}Frozen thermal conductivity 0.92 W m^{-1} K^{-1}Thawed volumetric heat capacity 2.300×10^6 J m^{-3} K^{-1}Frozen volumetric heat capacity 1.328×10^6 J m^{-3} K^{-1}Volumetric water content 45 %Mineral soilDepth >0.2 mThawed thermal conductivity 1.50 W m^{-1} K^{-1}Frozen thermal conductivity 2.26 W m^{-1} K^{-1}Thawed volumetric heat capacity 2.500×10^6 J m^{-3} K^{-1}Frozen volumetric heat capacity 1.852×10^6 J m^{-3} K^{-1}Volumetric water content 30 %

The numerical model was solved using an implicit finite-difference scheme for a 100 m deep domain, which was discretized so that the computation nodes were closely spaced in the active layer and shallow permafrost for the most accurate outputs there, while their density decreased towards the deepest node where the temperature remained stable. Specifically, the node spacing was 0.01 m, 0.1 m, 0.5 m, and >1 m, 5 m and 10 m in the depth intervals of 0–2 m, 2–5 m, 5–10 m, 10–20 m, 20–50 m and 50–100 m, respectively. At the upper boundary, the model was forced by the ground surface temperatures. A zero heat flux was set at the lower boundary. The initial temperature was established by Eq. (1) using thawing and freezing indices at the ground surface and at the bottom of the top peat layer for the one- and two-layer profiles, respectively, in order to speed up the time to reach the steady-state conditions throughout the model domain. The model was run for 50 years with a time step of 1 hour to ensure that the simulated temperatures are not affected by the initial conditions. Steady-state MAPT, ALT, and thawing and freezing indices simulated for the last year were then used for numerical validations of ASMs given by Eq. (8)and (27). While this requirement excluded numerous sites, it ensured that the benchmark values for MAPT and ALT could be established as accurately as possible.

3.1 Field observations

Ground temperatures were collected for 17 sites situated in permafrost environments on James Ross Island and McMurdo Sound in Antarctica and on the North Slope of Alaska in the Arctic (Table 2)in order to test ASMs under diverse climates and ground physical conditions. A total of 142–192 and 162–210 yearsWe collected ground temperature data for a total of 43 sites from monitoring networks and public databases of the Polar-Geo-Lab of the Masaryk University (MU) (e.g., Hrbáček et al., 2017a, b; Hrbáč , Global Terrestrial Network for Permafrost (GTN-P; http://gtnpdatabase.org), Natural Resources Conservation Service of the United States Department of Agriculture (USDA; https://www.nrcs.usda.gov/resources/data-and-reports/soil-climate-research-stations), Geophysical Institute Permafrost Laboratory of the University of Alaska Fairbanks (GI-UAF, https://permafrost.gi.alaska.edu), and National Tibetan Plateau/seasons (Table 2) with quality-checked observations of MAPT, ALT, and thawing and freezing indices were available for individual validation scenarios of ASMs given Eq. (8) and (27), respectively , (see Sect. **??**). The variability in the number of available yearsThird Pole Environment Data Center (NTP/seasons for the validations (Table 2)was because in some years/seasons the active layer was thinner than the deepest sensors used in Eq. (8) and (27) and/or due to data gaps.

List of the Antarctic and Alaskan sites and the number of years/seasons used for the model validations. Site Latitude [°] Longitude [°] Altitude [m asl] Validation period Years for MAPT Seasons for ALT James Ross IslandAbernethy Flats TPEDC; https://data.tpdc.ac.cn/en/disallow/789e838e-16ac-4539-bb7e-906217305a1d) (Zhao et al., 2017). The dataset comprised five different ground surface covers and three permafrost zones, spanned variable time periods during 1997–2023, and exhibited a wide range of MAPT and ALT from ~−63.88138 −57.94832 41 2013–2020 6–6 7–7Berry Hill slopes −63.80267 −57.83863

~~56 2017–2020 3–3 3–3CALM −63.80190 −57.88460 10 2014–2023 7–7 8–8Johann Gregor Mendel −63.80152 −57.88330 10 2011–2023 10–12 11–12Johnson Mesa −63.82250 −57.93280 340 2012–2023 8–11 9–11McMurdo SoundBull Pass −77.51847 161.86269 141 1999–2022 15–22 14–22Granite Harbour −77.00655 162.52561 6 2007–2017 4–4 5–5Marble Point −77.41955 163.68247 47 1999–2022 18–22 17–21North Slope of AlaskaAtqasuk 70.45242 −157.41178 22 1998–2010 6–9 8–12Barrow (site 1) 71.32242 −156.61089 9 1997–2017 15–16 15–17Betty Pingo: polygon center 70.28258 −148.89347 12 2006–2022 0–9 0–9Betty Pingo: polygon rim 70.28258 −148.89347 12 2006–2012 4–7 4–7Westdock (high): polygon center 70.37039 −148.56867 3 2002–2020 16–17 18–19Westdock (high): polygon rim 70.37039 −148.56867 3 2003–2020 16–17 18–18Westdock (high): polygon trough 70.37039 −148.56867 3 2003–2020 9–17 11–18Westdock (low): polygon center 70.37047 −148.56561 2 2004–2011 4–4 8–8Westdock (low): polygon trough 70.37047 −148.56561 2 2004–2022 1–9 6–13~~19 °C to ~0 °C and ~40 cm to ~300 cm, respectively (Table C1).

3.1 ~~Model evaluation~~

~~For both numerical and field validations of ASMs, the thawing and~~ Ground temperature data were first checked for quality and then daily means were calculated for all available depths before further processing. Thawing and freezing indices were calculated as annual sums of positive and negative mean daily ground temperatures, respectively, ~~and for convenience expressed in degree-days and in absolute values . textrmALT was derived~~ which were expressed in absolute values for convenience. ALT was determined as the maximum ~~seasonal~~ annual depth of the 0 °C isotherm ~~by a~~ that was tracked by linear interpolation of ~~the depths where the~~ mean daily ground temperatures ~~were just above and below 0 C. Subsequently,~~ within the measured profile. MAPT was calculated as the mean annual ~~temperatures at the same depths were used to interpolate MAPT. We used three pairwise combinations of thawing and freezing indices at the depth of 5 cm, 30 cm and 50 cm as inputs of~~ ground temperature, which was linearly interpolated to the depth that corresponds to ALT (e.g., Hrbáček et al., 2020, 2021; Kňažková and Hrbáček, 2024) . Hereafter, these values are referred to as the observed MAPT and ALT.

Subsequently, MAPT and ALT were also modelled using ASMs given by Eq. (8) and (27) ~~for numerical validations, while~~ forced by the measured thawing and freezing indices from the depth intervals of 0–10 cm, 25–35 cm and 45–55 cm~~(for convenience hereafter also referred to as~~ , which were combined into three pairs of 5/30 cm, ~~30~~5/50 cm and 30/50 cm ~~) were considered for field validations because the sensor depths differ at individual sites. However, this did not compromise the consistency of field validations and allowed us to reveal~~ so that they were comparable across the validation sites. This provided us with three sets of MAPT and ALT estimates that allowed to determine which depth combinations ~~and in which portion of the active layer~~ worked best. ~~The ASMs outputs were compared with~~

We compared the modelled MAPT and ALT ~~from the numerical model simulations and field observations and evaluated~~ directly with the observed MAPT and ALT, and evaluated the model accuracy for each site using common error metrics, such as ~~the~~ mean error (ME), ~~the~~ mean percentage error (MPE), ~~the~~ mean absolute error (MAE), ~~the~~ mean absolute percentage error (MAPE), and ~~the~~ root-mean-square error (RMSE). The evaluation statistics were grouped by depth pairs and surface cover, as the latter also broadly captures the common characteristics of the validation sites in terms of climate and composition of the active layer.

4 Results

4.1 Mean annual permafrost table temperature

4.1.1 ~~Numerical validation~~

~~The numerical model simulations for the five MAAT scenarios showed that the thawing and freezing indices tend to decrease exponentially from the ground surface towards the base of the active layer where the thawing indices are zero (Fig. 1). However, the relationships between the thawing and freezing indices themselves are linear within each subsurface layer (both peat and mineral soil), and their slopes are governed by the thermal conductivity ratios in the individual layers (Fig. 2).~~

~~Depth profiles of (A) the thawing indices and (B) the freezing indices in the active layer and near-surface permafrost simulated by the numerical model for MAAT of −12 C, −10 C, −8 C, −6 C and −4 C that varied sinusoidally over a year within a range of 40 C. Note the bent shapes of the thawing and freezing indices in the active layer, which only change abruptly at the interface of peat and mineral soil in the two-layer profiles due to distinct physical properties of these materials (see Table 1).~~

~~Relationships between the thawing and freezing indices in the active layer simulated by the numerical model for MAAT of −12 C, −10 C, −8 C, −6 C and −4 C that varied sinusoidally over a year within a range of 40 C. Note that the relationships are linear, but their slopes change abruptly at the interface of peat and mineral soil in the two-layer profiles due to distinct physical properties of these materials (see Table 1).~~

~~MAPT estimated~~ The MAPT modelled using ASM given by Eq. (~~8~~8) based on the ~~numerically modelled~~ measured thawing and freezing indices ~~at~~ for the depth pairs of 5/30 cm, 5/50 cm and 30/50 cm ~~for the five MAAT scenarios showed almost perfect agreement with MAPT simulated by the numerical model in the one-layer profiles (Table ??), as ME was −0.003~~showed the total site-weighted ME from 0.01 °C to ~~−0.002~~0.05 °C ~~, MAE was 0.002~~compared to the observed MAPT (Table 1). Since the errors were scattered around zero (Fig. 1), the total site-weighted MAE was somewhat larger and ranged from 0.11 °C ~~C to 0.003 C, and RMSE was 0.002 C to 0.003 C. The accuracy of Eq. (8)was slightly lower in the two-layer profiles (Table ??), as ME was −0.105~~ C to ~~−0.003~~0.16 °C, ~~MAE was 0.003~~while the total site-weighted RMSE was 0.12 °C to ~~0.105~~0.19 °C ~~, and RMSE was 0.004~~(Table 1). The majority of errors were within ±0.2 °C ~~to 0.124 C.~~(Fig. 1).

~~Overall, however, these findings corroborate the theoretical assumptions outlined in Sect. 2.1 and justify ASM given by Eq. (8) for estimating MAPT under the idealized scenarios.~~

4.1.1 ~~Field validation~~

~~MAPT estimated by Eq. (8) based on the thawing and freezing indices at the depth pairs~~The accuracy of the modelled MAPT was similar for the three depth pairs, although 5/~~30 cm, 5/~~50 cm and 30/50 cm ~~at the Antarctic and Alaskan sites yielded the site-weighted ME of 0.02~~performed slightly better than 5/30 ~~C to 0.03 C compared to the observed MAPT (Fig. 3). Since the errors were scattered around zero~~ cm (Table 1). Similarly, there were rather small differences between individual surface covers (Fig. ~~3) ,~~ 1) that exhibited the site-weighted ~~MAE was somewhat larger of 0.08~~ME from −0.06 °C to ~~0.14~~0.12 °C ~~and the site-weighted RMSE was 0.10 C to 0.17 C (Fig. 3). The majority of the errors was within 0.2 C (Fig. 3).~~

Table 1. Comparison Evaluation statistics of MAPT simulated by the numerical model for MAAT of −12 C, −10 C, −8 C, −6 C and −4 C that varied sinusoidally over a year within a range of 40 C and MAPT estimated with modelled using ASM given by Eq. (8) based on the numerically modelled measured thawing and freezing indices at for the depth pairs of 5/30 cm, 5/50 cm and 30/50 cm and diverse surface covers.

Scenario Depth pair	MAAT Surface cover	Sites	$MAPT_{obs}$ [°C]	$MAPT_{num\,mod}$ [°C]	$MAPT_{5/30}$ ME [°C]	$MAPT_{5/50}$ MAE [°C]	M
One layer 5/30 cm	−4 Bedrock	−1.24 2	−1.58	−1.25 1.59	−1.25 0.01	0.07	
	Bare	14	−8.84	−1.25 8.81	0.03	0.22	
	Grass	10	−5.80	−5.78	0.02	0.15	
	Shrub	6	−2.12	−2.38 2.14	−2.38 0.02	−2.38 0.06	
	−8 Forest	−3.50 5	−0.53	−3.51 0.54	−3.51 0.01	−3.51 0.19	
	−10 Total	−4.62 37	−5.41	−4.62 5.40	0.01	0.16	
5/50 cm	Bedrock	2	−1.57	−4.62 1.59	−4.62 0.02	0.16	
	Bare	14	−8.84	−8.77	0.07	0.13	
	Grass	12	−5.73 4.50	−5.73 4.56	−5.73 0.06	−5.73 0.12	
	Mean Shrub	−3.49 6	−3.50 2.12	−3.50 2.12	−3.50 0.00	0.04	
Two layers	−4 Forest	−1.51 5	−1.72 0.52	−1.63 0.55	−1.52 0.03	0.08	
	−6 Total	−2.62 39	−2.77 5.03	−2.70 5.03	−2.62 0.00	0.11	
30/50 cm	−8 Bedrock	−3.72 4	−2.88	−3.81 2.76	−3.76 0.12	−3.72 0.23	
	Bare	14	−8.83	−8.74	0.09	0.14	
	Grass	10	−4.81 5.35	−4.86 5.33	−4.83 0.02	−4.81 0.07	
	−12 Shrub	−5.88 6	−2.12	−5.90 2.12	−5.88 0.00	−5.88 0.04	
	Mean Forest	5	−0.52	−3.71 0.53	−3.81 0.01	0.07	
	Total	39	−3.76 5.23	−3.71 5.18	0.05	0.11	

(Upper row) Comparison of MAPT observed at the Antarctic and Alaskan sites and MAPT estimated with ASM given by Eq. (8) based on the observed thawing and freezing indices at the depth pairs of 5/30 cm, 5/50 cm and 30/50 cm. The blue and green numbers in parentheses indicate the mean errors for the Antarctic and Alaskan sites, respectively. The black solid and dashed lines represent the line of identity and the deviation of 1 C, respectively. (Lower row) Probability distribution of the errors in MAPT estimated with ASM for the depth pairs of 5/30 cm, 5/50 cm and 30/50 cm.

The accuracy of the ASM estimates was slightly lower in Antarctica (Fig. 3) where the site-weighted ME was −0.04 C to 0.04 C, (Table 1). However, the MAPT estimates were somewhat better at the vegetated sites, as the site-weighted MAE was 0.10 C to and RMSE there were mostly less than ~0.15 °C, and the site-weighted RMSE was 0.13 Cto 0.18 C. In Alaska, , while the bedrock and bare-ground sites mostly showed the site-weighted ME was −0.01 C to 0.09 C, the site-weighted MAE was 0.07 C to 0.13 C, and the site-weighted RMSE was 0.08 C to and RMSE greater than ~0.15 °C . However, the ASM deviations

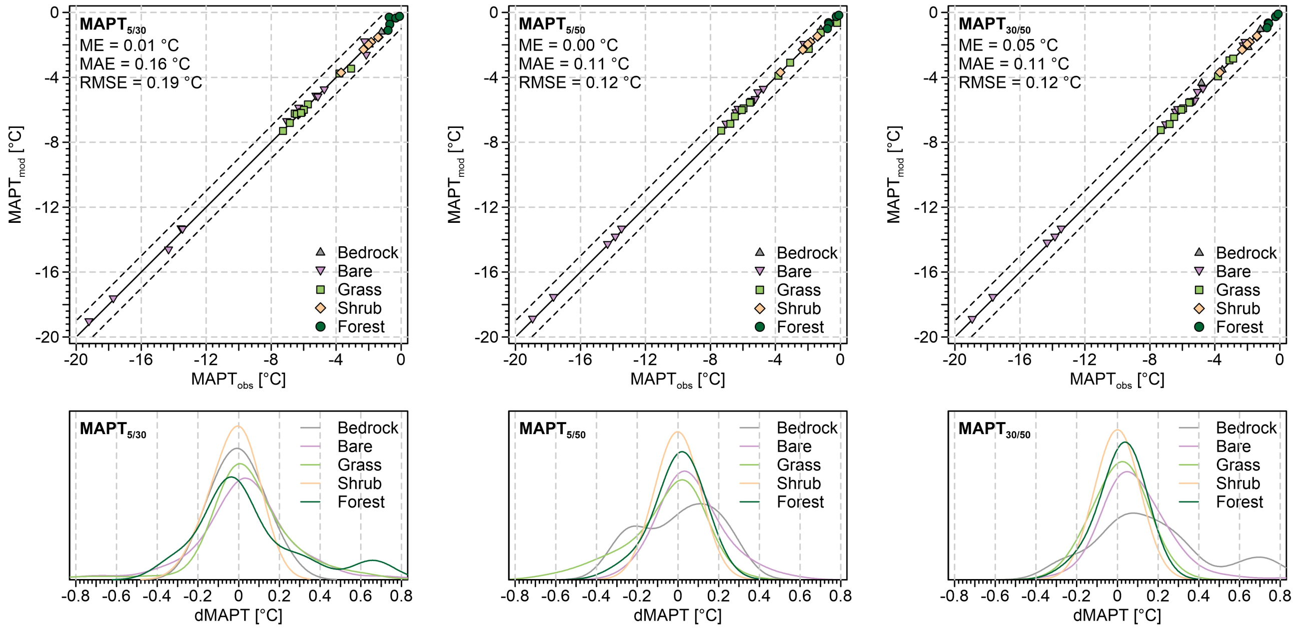

Figure 1. Comparison of the observed MAPT and MAPT modelled using ASM given by Eq. (8) based on the measured thawing and freezing indices for the depth pairs of 5/30 cm, 5/50 cm and 30/50 cm and diverse surface covers. The black solid and dashed lines in the upper plots represent the line of identity and the deviation of ±1 °C, respectively.

~~exhibited very similar distributions in both regions (Fig. 1).~~ (Table 1). The site-weighted errors also tended to be somewhat larger at higher MAPT for all three depth pairs.

4.2 Active-layer thickness

4.2.1 ~~Numerical validation~~

~~As stated in Sect. ??, the numerical model simulations for the five MAAT scenarios showed that the thawing indices tend to decrease exponentially from the ground surface towards the base of the active layer where they are zero (Fig. 1A). If square rooted, however, the bent-shaped depth profiles of the thawing indices become linear within each subsurface layer (both peat and mineral soil), except for subtle deviations near the base of the active layer, and their slopes are governed by the edaphic terms in the individual layers (Fig. 4).~~

~~Depth profiles of the square-rooted thawing indices in the active layer and near-surface permafrost simulated by the numerical model for MAAT of −12 C, −10 C, −8 C, −6 C and −4 C that varied sinusoidally over a year within a range of 40 C. Note that the bent shapes of the thawing indices (Fig. 1A) become linear when square-rooted, but their slopes change abruptly at the interface of peat and mineral soil in the two-layer profiles due to distinct physical properties of these materials (see Table 1).~~

Table 2. ~~Comparison~~ Evaluation statistics of ALT ~~simulated by the numerical model for MAAT of −12 C, −10 C, −8 C, −6 C and −4 C that varied sinusoidally over a year within a range of 40 C and ALT estimated with~~ modelled using ASM given by Eq. (27) based on the ~~numerically modelled~~ measured thawing and freezing indices ~~at~~ for the depth pairs of 5/30 cm, 5/50 cm and 30/50 cm and diverse surface covers.

~~Scenario~~ Depth pair	~~MAAT~~ Surface cover	Sites	ALT_{obs} [~~C~~cm]	ALT ~~num~~ mod [cm]	~~$ALT_{5/30}$~~ ME [cm]	~~$ALT_{5/50}$~~ MPE [%]	MAE [cm]
~~One layer~~ 5/30 cm	~~−4~~ Bedrock	~~195~~ 2	~~193~~ 116.8	~~194~~ 154.8	~~195~~ 38.0	33.8	38.0
	~~−6~~ Bare	~~170~~ 14	~~170~~ 85.1	~~170~~ 89.1	~~171~~ 4.0	4.3	11.3
	~~−8~~ Grass	~~146~~ 10	~~147~~ 62.1	~~148~~ 58.2	−3.9	~~148~~ −7.8	7.6
	Shrub	6	64.3	44.2	−20.1	−~~10~~ 31.0	~~123~~ 20.1
	~~126~~ Forest	5	89.3	51.2	−38.1	−34.6	38.1
	Total	37	77.8	71.9	−~~12~~ 5.9	~~100~~ −8.3	~~103~~ 16.8
5/50 cm ~~Two layers~~	~~Mean~~ Bedrock	~~146.8~~ 2	~~147.6~~ 116.8	~~148.2~~ 119.4	~~148.6~~ 2.6	2.0	9.0
	~~−4~~ Bare	~~157~~ 14	~~90~~ 86.3	~~116~~ 90.7	~~158~~ 4.4	2.4	9.1
	Grass	12	103.2	87.4	−15.8	−10.1	18.6
	Shrub	6	~~133~~ 64.3	~~79~~ 57.7	~~102~~ −6.6	~~134~~ −10.3	6.6
	Forest	5	89.4	63.8	−25.6	−~~8~~ 17.7	~~109~~ 25.7
	~~112~~ Total	39	90.1	82.6	−7.5	−6.0	13.8
30/50 cm	Bedrock	4	184.8	176.7	−8.1	−1.4	27.9
	Bare	14	86.4	93.2	6.8	3.7	11.4
	Grass	10	~~87~~ 76.5	~~59~~ 80.1	~~75~~ 3.6	~~90~~ 1.0	8.7
	Shrub	6	64.3	62.8	−1.5	−~~12~~ 2.5	~~65~~ 3.8
	~~69~~ Forest	5	89.4	72.2	−17.2	−10.8	18.1
	~~Mean~~ Total	~~110.2~~ 39	~~69.2~~ 90.9	~~88.6~~ 91.0	~~112.6~~ 0.1	−0.3	12.1

~~ALT estimated~~ The ALT modelled using ASM given by Eq. (27) based on the ~~numerically modelled thawing indices at~~ measured thawing indices for the depth pairs of 5/30 cm, 5/50 cm and 30/50 cm ~~for the five MAAT scenarios was well consistent with ALT simulated by the numerical model in the one-layer profiles (Table ??), as ME was 0.8~~exhibited the total site-weighted ME from −7.5 cm (~~0.9~~−8.3 %) to ~~1.8~~0.1 cm (~~1.5~~−0.3 %) ~~, MAE was 1.6~~compared to the observed ALT (Table 2). The total site-weighted MAE was larger (Fig. 2) and reached 12.1 ~~cm (1.3 %) to 1.8 cm (1.5 %), and RMSE was 1.6 cm to 1.9 cm. On the other hand, the accuracy of Eq. (27) was much worse in the two-layer profiles when the thawing indices from the top peat layer were used for the calculations (Table ??), as ME was −41.0 cm (−35.4 %) to 2.4~~ cm (~~2.7~~9.7 %) ~~, MAE was 2.4~~to 16.8 ~~cm (2.7 %) to 41.0~~ cm (~~35.4~~19.3 %), ~~and RMSE was 3.4~~while the total site-weighted RMSE was 13.2 cm to ~~35.9~~18.0 cm ~~. The deviations tended to decrease as the active layer thickened in the one-layer profiles, while they tended to increase as the active-layer thickened in the two-layer profiles~~ (Table ~~??~~2).

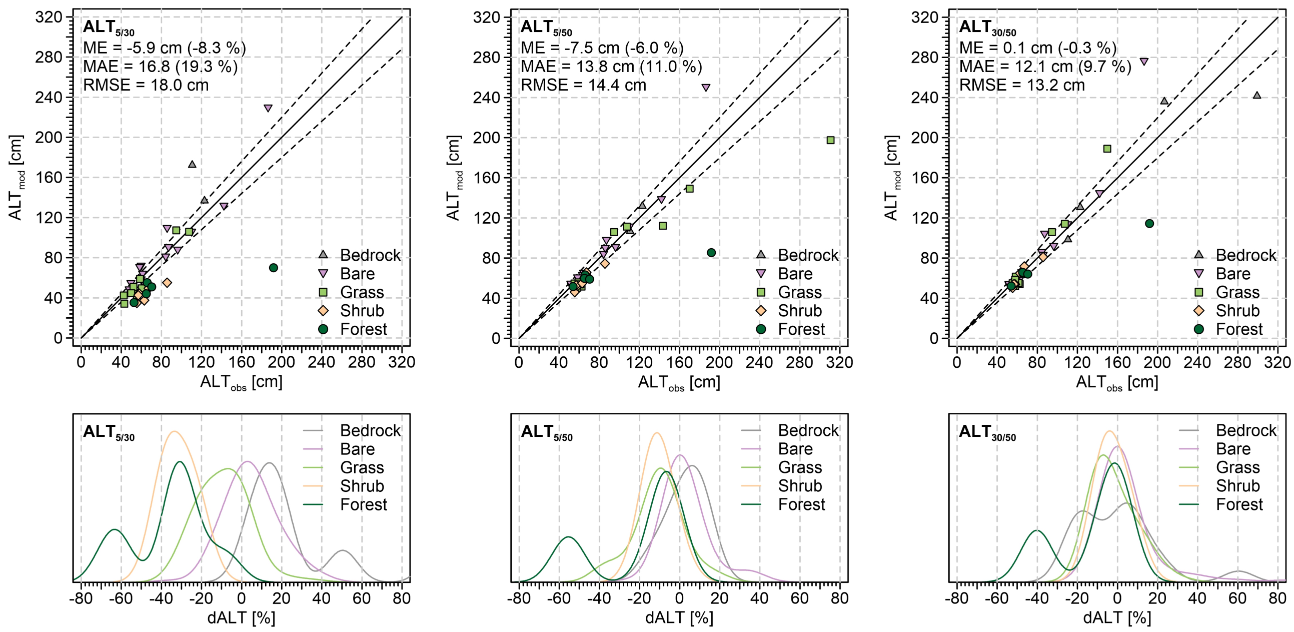

Figure 2. Comparison of the observed ALT and ALT modelled using ASM given by Eq. (27) based on the measured thawing and freezing indices for the depth pairs of 5/30 cm, 5/50 cm and 30/50 cm and diverse surface covers. The black solid and dashed lines in the upper plots represent the line of identity and the deviation of ±10 %, respectively.

Overall, however, these findings corroborate the theoretical assumptions outlined in Sect. 2.2 and justify ASM given by Eq. (27) for estimating ALT under idealized scenarios in one-layer profiles.

4.2.1 Field validation

ALT estimated by Eq. (27) based on the thawing indices at the The accuracy of the modelled ALT was higher for the depth pairs of 5/30 cm, 5/50 cm and 30/50 cm at the Antarctic and Alaskan sites showed the site-weighted ME of −2.6compared to 5/30 cm (−4.4 %)to −1.4 cm (−2.4 %) compared to the observed ALT (cm, especially at the bedrock, shrub and forest sites (Table 2). Additionally, there were rather large differences between individual surface covers (Fig. ??). The 2), among which the site-weighted MAE was somewhat larger, as it attained 4.8ME ranged from −38.1 cm (6.9–34.6 %) to 8.838.0 cm (13.533.8 %) , while the (Table 2). The most accurate ALT estimates were at the bare-ground sites and those with grass and shrub cover, as their site-weighted RMSE was 5.3 cm to 9.8 cm (Fig. ??).

(Upper row) Comparison of ALT observed at the Antarctic and Alaskan sites and ALT estimated with ASM given by Eq. (27) based on the observed thawing indices at the depth pairs of 5/30 cm, 5/50 cm and 30/50 cm. The blue and green numbers in parentheses indicate the mean errors for the Antarctic and Alaskan sites, respectively. The black solid and dashed lines represent the line of identity and the deviation of 10 %, respectively. (Lower row) Probability distribution of the errors in ALT estimated with ASM for the depth pairs of 5/30 cm, 5/50 cm and 30/50 cm.

ALT estimates by Eq. (27) were more accurate in Antarctica where the site-weighted ME was 0.9 cm (0.8 %) to 5.4 cm (7.2 %), the site-weighted MAE was 3.5ranged from 3.8 cm (4.66.0 %) to 8.420.1 cm (11.931.0 %), and the site-weighted RMSE was 4.0from 3.8 cm to 9.720.3 cm . By contrast, in Alaska the site-weighted ME was −8.6 cm (−13.9 %)to −3.6 cm (−5.6 %), (Table 2). Somewhat worse was the model performance at the bedrock and forest sites, with the site-weighted MAE was 5.2from 9.0 cm (8.27.9 %) to 9.138.1 cm (14.934.6 %) , and the site-weighted RMSE was 5.8from 10.4 cm to 10.043.4 cm . The ASM deviations were roughly scattered around zero in Antarctica, while they tended to be negative in Alaska where the deviations also exhibited a bimodal distribution for the depth pair of 5/30 cm (Fig. ??). (Table 2). The site-weighted errors were also larger at thicker ALT for all three depth pairs.

5 Discussion

5.1 Model performancesMean annual permafrost table temperature

ASMs given by Eq. (8) and (27) reproduced MAPT and ALT with a reasonable accuracy under most idealized scenarios and field conditions, which corroborated their theoretical assumptions (see Sect. 2.1 and 2.2) and suggested that they can work reasonably well under a wide range of climates and ground physical conditions.

5.1.1 Mean annual permafrost table temperature

MAPT estimates by Eq. (8) had high accuracy regardless of the stratigraphy of the active layer and the depth pairs used for the calculations (Table ??, The modelled MAPT showed a relatively high accuracy for all three depth pairs and surface covers (Fig. 3). Under idealized scenarios, the ASM deviations in the one-layer profiles were negligible, while in the two-layer profiles the temperatures were underestimated by less than ~0.1 C on average (Table ??). Under field conditions, the ASM deviations were 1), with the mean errors close to zero on average, and the majority of them was below within ±0.2 °C at the Antarctic and Alaskan sites (Fig. 3(Table 1), which is within the accuracy of many temperature sensors and similar or better than in most previous studies that used other analytical or statistical models for MAPT estimates (e.g., Romanovsky and Osterkamp, 1995; Sazonova and R . This is likely because the relationship between the thawing and freezing indices is linear within each subsurface layer , and its slope varies rather slightly with vertical changes in ground physical properties at the layer interfaces (Fig. 2). This was noticeable at the Alaskan sites where the presence of peat over mineral soil is common. (e.g., Romanovsky and Osterkamp, 1995; Sazonova .

Somewhat larger errors in the modelled MAPT arose especially under warmer conditions and within a thicker active layer where MAPT needs to be extrapolated to greater depth. Warmer climates are also dominated by vegetated sites (Table C1) with well-developed soils and therefore a more heterogeneous active layer where MAPT estimates are more difficult. In addition, it may also be associated with increased complexity of the system at permafrost temperatures approaching 0 °C when simple models tend to fail to a greater extent (Riseborough, 2007). The worst MAPT estimates at the bedrock sites were also likely

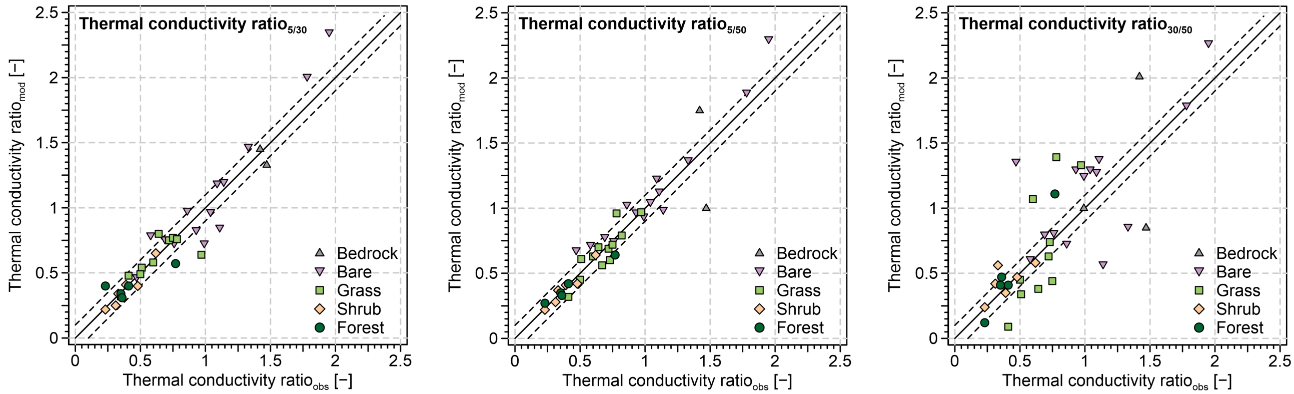

Figure 3. Comparison of the observed thermal conductivity ratio for the whole active layer and thermal conductivity ratio estimated using Eq. (5) based on the measured thawing and freezing indices for the depth pairs of 5/30 cm, 5/50 cm and 30/50 cm and diverse surface covers. The black solid and dashed lines represent the line of identity and the deviation of ±0.1.

because active layer is thick there (Table 1). Moreover, the boreholes were drilled into vertical rockwalls, and therefore it is possible that lateral flows of heat and moisture occur in the fractured bedrock, which further complicates MAPT estimates.

So far, ~~MAPT models have also~~ models for estimating MAPT have typically assumed that ~~thawed~~ the ratio of thawed and frozen thermal conductivity is ~~lower than frozen one~~less than or equal to 1, and that the thermal offset is therefore ~~negativ~~ negative (e.g., Gisnås et al., 2013; Obu et al., 2019, 2020), which would ~~, however, yield~~ result in invalid MAPT estimates ~~under reverse conditions . Since Eq. (8)utilizes measured temperatures, it can easily handle even such anomalies, as demonstrated , for example, in McMurdo Sound where the thermal offset is often positive (?).Additionally, the thermal offset is usually in the order of tenths to first degrees Celsius and decreases exponentially with depth (Goodrich, 1982; Burn and Smith, 1988; Romanovsky and Osterka .Hence, it was relatively small below the bottom temperature sensors used for the calculations and MAPT estimates were subject to relatively small uncertainties. Somewhat larger deviations in MAPT estimates would, however, be expected in warmer conditions with thicker active layers and high~~ if the actual conditions were reversed. However, although nearly half of the bedrock and bare-ground sites exhibited a positive thermal offset with a thermal conductivity ratio above 1, the MAPT was modelled with similar accuracy at these locations as elsewhere (Table 1, Fig. 1). This is because ASM utilizes measured thawing and freezing indices within the active layer and can therefore easily capture this behaviour. This is also demonstrated by the thermal conductivity ratios modelled using Eq. (5) for the three depth levels that are close to those for the whole active layer (Fig. 3), which is likely because the relationship between the thawing and freezing indices within the active layer is linear (see Sect. 2.1) and its slope varies rather slightly with vertical changes in ground physical properties.

5.1.1 ~~Active-layer thickness~~

~~By contrast, ALT estimates by Eq. (27) had very different accuracy in the one-layer and two-layer profiles that also depended on the depth pairs used for the calculations (Table ??,~~

5.2 Active-layer thickness

Unlike MAPT, the modelled ALT showed variable performance for individual depth pairs and surface covers (Fig. ~~??). Under idealized scenarios, the ASM deviations in the one-layer profiles were below 1.5~~2, Table 2). However, the errors were mostly well within ±20 %~~on average, while in the two-layer profiles the deviations were up to tens of percent, except~~ , which is also similar or better than in most previous studies that used other analytical or statistical models for ALT (Anisimov et al., 1997; Nelson et al., 1 .

Notably, the modelled ALT showed variable accuracy for the depth pair of ~~30~~5/~~50~~30 cm ~~, which excluded the thawing index from the top peat layer with different physical properties~~ (Table ~~??). The minor deviations in the one-layer profiles and in the two-layer profiles for the depth pair of 30/50 cm were largely because the vertical profiles of the square-rooted thawing indices were not perfectly linear near the base of the active layer (Fig. 4), which was likely due to upward freezing from the permafrost table at the end of the thawing seasons (cf. Riseborough, 2003). Under field conditions, the ASM deviations were scattered around zero at the Antarctic sites and roughly attained less than 7 % on average, while ALT tended to be underestimated at the Alaskan sites by up to 14 % on average~~ 2). This is because the active layer is typically more heterogeneous at the vegetated sites and may often comprise a surface organic layer there, the physical properties of which strongly differ from the ground underneath. This alters the temperature gradient within the active layer and results in worse ALT estimates, which can be observed especially at the shrub and forest sites (Fig. ~~??). Overall, however, the accuracy of ASM given by Eq. (27)was similar or better than in most previous studies that used the other analytical or statistical models for ALT estimates (Anisimov et al., 1997; Nelson et al., 1997; Romanovsky and Osterkamp, 1997; Anisimov et al., 2002; Shiklomanov and Nelson, 2002; S~~ ~~. The higher accuracy of ASM at the Antarctic sites (Fig. ??)was likely due to the fact that the~~ 2). By contrast, the ALT estimates showed substantially lower errors for the depth pairs of 5/50 cm and 30/50 cm (Fig. 2), which largely to completely eliminated the influence of the surface layer. This also explains the consistently high accuracy of the modelled ALT at the bare-ground sites for all three depth pairs (Table 2), as the active layer there is relatively homogeneous in terms of its stratigraphy and physical properties~~, whereas at the Alaskan sites it typically consists of two distinct layers.This is also why the depth pair of 30/50 cm showed the lowest errors~~ . The ALT estimates were also relatively accurate at the bedrock sites (Table 2), but the same concern exists for them as for MAPT (see Sect. 5.1.1). Similarly to MAPT, the modelled ALT tended be less accurate under warmer conditions dominated by vegetated sites with a more heterogeneous and thick active layer (Table C1) where ALT needs to be extrapolated to greater depth.

Previous studies have estimated the edaphic term based on the relationship between ALT and thawing index (Nelson and Outcalt, 1987; H , which is restrictive, as it requires ALT. However, the edaphic term modelled using Eq. (20) for the three depth levels was close to the edaphic term calculated for the whole active layer (Fig. ~~??), as it excluded the surface layer of peat, which is an effective thermal insulator that substantially alters the temperature gradient in~~ 4). As with MAPT, this is because the square root of the thawing index within the active layer ~~.~~ is linear (see Sect. 2.2) and its slope varies rather slightly with vertical changes in ground physical properties (Riseborough, 2003).

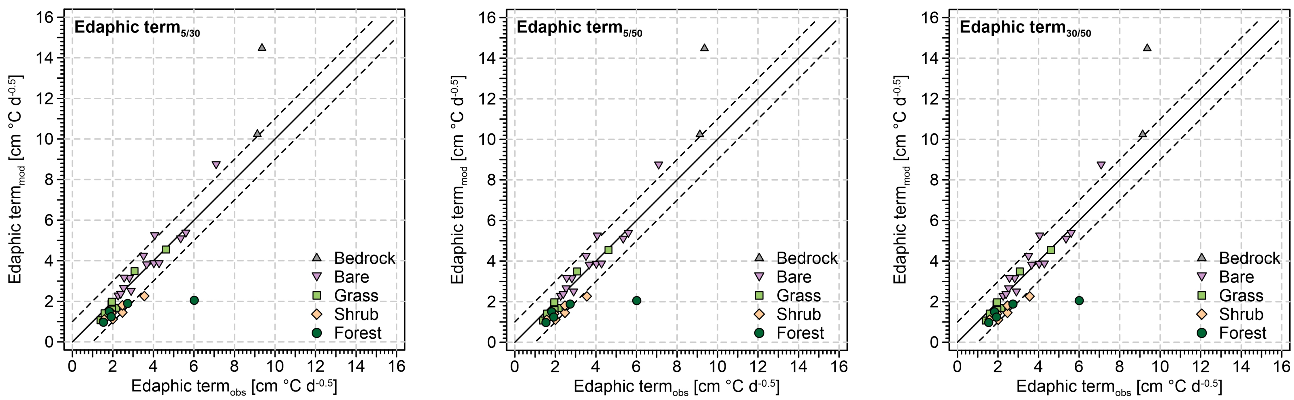

Figure 4. Comparison of the observed edaphic term for the whole active layer and edaphic term estimated using Eq. (20) based on the measured thawing and freezing indices for the depth pairs of 5/30 cm, 5/50 cm and 30/50 cm and diverse surface covers. The black solid and dashed lines represent the line of identity and the deviation of ±1 cm °C $d^{-0.5}$.

5.3 Model advantages

Unlike other analytical or statistical models for estimating MAPT (e.g., Garagulya, 1990; Romanovsky and Osterkamp, 1995; Smith and Riseborough, 1996) and ALT (e.g., Neumann, c. 1860; Stefan, 1891; Kudryavtsev et al., 1977), ASMs given by Eq. (8) and (27) can be utilized in any substrates work in any grounds where conductive heat transfer prevails , such as soil, peat, or solid rock, without the knowledge of without knowing their physical properties. Since ASMs build solely on

Although ASMs utilize only thawing and freezing indices at two distinct depths in from two depth levels within the active layer , the values of which reflect the rate of heat transfer across their intermediate layer, the solutions also intrinsically as inputs, they inherently account for the temporal natural variability of ground physical properties . Likewise, they in the intermediate layer between these two depths. Similarly, ASMs consider latent and sensible heat and any other factors that might affect the or other factors there, although these are not explicitly accounted for. This is because the relative values of the thawing and freezing indices at the two depth levels reflect the rate of heat transfer in the active layer , some of which other models do not explicitly account for. intermediate layer between them (see Eq. 5 and 20) that is influenced by seasonal changes in ground physical properties. So in principle it is analogous to, for instance, the calculations of apparent thermal diffusivity, which are based on damping of temperature amplitude or phase lag between two depth levels (Horton et al., 1983).

This is highly convenient because data on ground physical properties, such as thermal conductivity, heat capacity, water content or bulk density, are not readily available at many sitesfrequently unavailable or unrepresentative. Ground physical properties for other models estimating MAPT (e.g., Gisnås et al., 2013; Obu et al., 2019, 2020; Garibaldi et al., 2021) and ALT (e.g., Hinkel and Nicholas, 1995; Nelson et al., 1997; Anisimov et al., 2002; Shiklomanov and Nelson, 2002) have been set empirically or have been in other models for MAPT and ALT have therefore been estimated empirically or based on published values , and therefore their values have frequently been of unknown validity with unknown validity (e.g., Hinkel and Nicholas, 1995; . Ground physical properties also commonly show more or less variability on seasonal and annual time scales (e.g., Gao et al., 2020; Hrbáček et al., 2023a; Li et al., 2023; Kňažková and Hrbáček, 2024; Wenhao et al., 2024), which most other models cannot handle because they typically treat ground physical properties as constants ~~.~~ for whole modelling periods. Of course, ASMs in principle also treat them as constants, but their values are representative for individual years (Eq. 8) or thawing seasons (Eq. 27), which is a major improvement over other analytical or statistical models for MAPT (e.g., Garagulya, 1990; Romanovsky and Oste and ALT (e.g., Neumann, c. 1860; Stefan, 1891; Kudryavtsev et al., 1977).

~~Another advantage is that ASMs are not limited to temperatures at certain depths, but~~ Therefore, we believe that in addition to MAPT and ALT estimates, ASMs could also be useful for investigating temporal and spatial variations in the thermal conductivity ratio (Fig. 3) and edaphic term (Fig. 4), which might be investigated using networks of miniature temperature loggers collecting data only in shallow parts of the active layer. This is because another advantage of ASMs is that their inputs can be any depth combinations from within the active layer~~based on temperature data availability and site characteristics. For best MAPT and ALT estimates, it is therefore suggested to use~~ . For most accurate outputs, however, we suggest using thawing and freezing indices from ~~depths~~ depth levels as close as possible to the permafrost table~~, where available~~. For instance, this could improve ALT estimates at the bedrock sites where active layer is thick.

~~Besides field measurements, ASMs can~~ In addition to *in situ* ground temperature measurements, we suppose that ASMs could also be forced by diverse climate ~~reanalysis or climate model outputs~~reanalyses or Earth system models, if these at least partially ~~consider~~ account for the physics of ground thawing and freezing. ~~These products~~ While these products have been widely used for permafrost applications (e.g., Cao et al., 2020; Kaplan Pastíriková et al., 2024; Liu et al., 2025), they typically provide only ground surface and shallow active-layer temperatures with ~~limited or no information on~~ ground physical properties largely unknown, which is frequently insufficient to determine MAPT and ALT ~~either~~ directly or using conventional ~~solutions. However, this is not an issue for ASMs~~ models. If the active layer is thick, MAPT and ALT have therefore usually been confined to the deepest ground temperature level available in these products, which can obviously be misleading (e.g., Cao et al., 2020) . However, ASMs are designed so that they should be able to provide MAPT and ALT estimates even under these conditions.

Lastly, ASMs can also be easily reformulated to be used for estimating the mean annual temperature at the base of seasonally frozen ground and frost depth (see Appendix A and B).

5.4 Model limitations

Since ASMs assume ~~homogeneous (one-layer) profiles, they may understate reality in multi-layer profiles that exhibit large stepwise~~ that active layer is vertically homogeneous, they can be biased if there are strong vertical changes in ground physical properties and/or higher ground-ice ~~contents~~ content near the base of the active layer (Riseborough, 2003). ~~If, for instance,~~ For instance, if temperature measurements are used ~~only from the top layer, the physical properties of which differ from those of the layer below~~from the topmost layer, whose physical properties differ from the rest of the active layer, ASMs may ~~therefore be inaccurate(Fig. 2 and 4). Equally, the outputs may have unknown validity~~ be inaccurate. Similarly, the modelled MAPT and ALT may be unreliable if only shallow temperature measurements in ~~thick active layers are usedbecause they~~ a thick active layer are used. This is because the estimates would be based on ~~the rate of heat transfer in a tiny~~ physical properties of a small portion of the active layer, which may ~~differ~~ be different in its deeper ~~sections (Fig. 2 and 4). On the other hand,~~ parts.

Nevertheless, the natural variability of ground physical properties ~~with no~~ without sharp changes in their vertical distribution is unlikely to ~~affect ASMs substantially.~~have a major influence on the MAPT and ALT estimates (see Fig. 1 and 2, Table 1 and 2).

Other downside of ASMs is that they require temperature measurements ~~at two depths in~~ from two depth levels within the active layer, which may not be available at many sites~~, and can also be problematic to collect if the active layer is thin. Special care must also be taken with the depths of the temperature sensors and the vertical distances between them, which must be constant over time, as well as with the accuracy of the sensors, because any deviations in these may negatively influence the ASMs outputs. Nevertheless, these issues are largely common to any analytical, statistical and even numerical permafrost models, as they relate to the quality of the inputs rather than the shortcomings of ASMs themselves.~~ .

6 Conclusions

We devised two novel ~~ASMs~~ analytical–statistical models (ASMs) for estimating MAPT and ALT given by Eq. (8) and (27)~~for estimating MAPT and ALT~~, respectively, which are driven solely by ~~pairwise combinations of~~ thawing and freezing indices ~~in~~ from two depth levels within the active layer~~;~~, while no ground physical properties are required. ASMs reproduced MAPT and ALT ~~well under most idealized scenarios, which corroborated their theoretical assumptions. Under field conditions of Antarctica and Alaska, the mean ASMs deviations in MAPT and ALT were less than 0.03~~in the Earth's major permafrost regions with the total mean errors of less than 0.05 °C and ~~5~~8 %, respectively, which is very promising because it is similar or better than other analytical or statistical models. ASMs worked best in ~~homogeneous active layers~~ a homogeneous active layer with small vertical changes in ground physical properties and when permafrost table was close below the temperature sensors considered for MAPT and ALT ~~calculations.~~ estimates. By contrast, they performed worst in a heterogeneous and thick active layer when the topmost organic layer influenced the estimates.

~~Hence, ASMs for estimating MAPT and ALT can find~~ We believe that ASMs can find useful applications under a wide range of climates, ground surface covers and ground physical conditions wherever at least two temperature measurements ~~in~~ within the active layer are available. ~~Besides field measurements ,~~They are primarily intended to be used for MAPT or ALT estimates where ground temperature measurements are too shallow and MAPT or ALT therefore cannot be determined directly, but they can also be used to establish typical values of the thermal conductivity ratio and the edaphic term for MAPT and ALT estimates in the past and in the future or for modelling their spatial variations. In addition to *in situ* measurements, they could utilize diverse climate reanalyses or ~~climate model ground temperature products~~Earth system models. Lastly, they can be easily reformulated for estimating the mean annual temperature at the base of seasonally frozen ground and frost depth.

Appendix A: Derivation of ASM for mean annual temperature at the base of seasonally frozen ground

Similarly to Eq. (1), the mean annual temperature at the base of seasonally frozen ground (MASFT $> 0\,^{\circ}$C) is calculated as follows (Romanovsky and Osterkamp, 1995)

$$\text{MASFT} = \frac{I_{ts} - \frac{k_f}{k_t} I_{fs}}{P}. \tag{A1}$$

~~which has the same attributes as Eq. (1). Hence,~~ MASFT based on temperatures measured at two distinct depths in the seasonally freezing layer z_1 and z_2 ($z_1 < z_1 <$ FD) can therefore be expressed as follows

$$\text{MASFT} = \frac{I_{tz_1} - \frac{k_f}{k_t} I_{fz_1}}{P}, \tag{A2}$$

$$\text{MASFT} = \frac{I_{tz_2} - \frac{k_f}{k_t} I_{fz_2}}{P}. \tag{A3}$$

This implies that Eq. (A2) and (A2) are equivalent:

$$\frac{I_{tz_1} - \frac{k_f}{k_t} I_{fz_1}}{P} = \frac{I_{tz_2} - \frac{k_f}{k_t} I_{fz_2}}{P}. \tag{A4}$$

Solving Eq. (A4) for the inverse of the thermal conductivity ratio yields

$$\frac{k_f}{k_t} = \frac{I_{tz_1} - I_{tz_2}}{I_{fz_1} - I_{fz_2}}. \tag{A5}$$

Equation (A5) can be then substituted for the thermal conductivity ratio in Eq. (A2) and (A3) as follows

$$\text{MASFT} = \frac{I_{tz_1} - \frac{I_{tz_1} - I_{tz_2}}{I_{fz_1} - I_{fz_2}} I_{fz_1}}{P}, \tag{A6}$$

$$\text{MASFT} = \frac{I_{tz_2} - \frac{I_{tz_1} - I_{tz_2}}{I_{fz_1} - I_{fz_2}} I_{fz_2}}{P}. \tag{A7}$$

Subsequently, Eq. (A6) and (A7) both simplify to the same formula for MASFT:

$$\text{MASFT} = \frac{\frac{I_{fz_1} I_{tz_2} - I_{fz_2} I_{tz_1}}{I_{fz_1} - I_{fz_2}}}{P}, \tag{A8}$$

which only slightly differs from Eq. (A8)~~and has the same attributes~~.

Appendix B: Derivation of ASM for frost depth

Similarly to Eq. (13), the frost depth (FD) can be calculated ~~by~~ using the Stefan (1891) model as follows

$$\text{FD} = \sqrt{\frac{2 k_f I_{fs}}{L \phi}}. \tag{B1}$$

~~Likewise~~As with Eq. (13), note that the freezing index must be multiplied by the scaling factor of 86 400 s d^{-1} ~~in the Stefan model to yield correct outputs~~. FD estimated using freezing indices measured at two distinct depths z_1 and z_2 ($z_1 < z_1 <$FD) can be expressed as follows

$$\mathrm{FD} = z_1 + \sqrt{\frac{2k_f I_{fz_1}}{L\phi}}, \tag{B2}$$

$$\mathrm{FD} = z_2 + \sqrt{\frac{2k_f I_{fz_2}}{L\phi}}. \tag{B3}$$

This implies that Eq. (B2) and (B3) are equivalent:

$$z_1 + \sqrt{\frac{2k_f I_{fz_1}}{L\phi}} = z_2 + \sqrt{\frac{2k_f I_{fz_2}}{L\phi}}. \tag{B4}$$

The vertical distance between z_2 and z_1 can be expressed as

$$z_2 - z_1 = \sqrt{\frac{2k_f I_{fz_1}}{L\phi}} - \sqrt{\frac{2k_f I_{fz_2}}{L\phi}}, \tag{B5}$$

which simplifies to

$$z_2 - z_1 = \sqrt{\frac{2k_f}{L\phi}} \left(\sqrt{I_{fz_1}} - \sqrt{I_{fz_2}}\right). \tag{B6}$$

Subsequently rearranging Eq. (B6) gives

$$\frac{z_2 - z_1}{\sqrt{I_{fz_1}} - \sqrt{I_{fz_2}}} = \sqrt{\frac{2k_f}{L\phi}}, \tag{B7}$$

where the right-hand side corresponds to the edaphic term, which combines the ground physical properties in the Stefan model into a single variable. The edaphic term can be implemented in Eq. (B2) and (B2) as ~~follows~~

$$\mathrm{FD} = z_1 + E\sqrt{I_{fz_1}}, \tag{B8}$$

$$\mathrm{FD} = z_2 + E\sqrt{I_{fz_2}}. \tag{B9}$$

Substituting the left-hand side of Eq. (B7) for the edaphic term in Eq. (B8) and (B9) yields

$$\mathrm{FD} = z_1 + \frac{z_2 - z_1}{\sqrt{I_{fz_1}} - \sqrt{I_{fz_2}}}\sqrt{I_{fz_1}}, \tag{B10}$$

$$\mathrm{FD} = z_2 + \frac{z_2 - z_1}{\sqrt{I_{fz_1}} - \sqrt{I_{fz_2}}}\sqrt{I_{fz_2}}. \tag{B11}$$

Simplifying Eq. (B10) and (B11) then produces the same formula for FD:

$$\mathrm{FD} = \frac{z_2\sqrt{I_{fz_1}} - z_1\sqrt{I_{fz_2}}}{\sqrt{I_{fz_1}} - \sqrt{I_{fz_2}}}, \tag{B12}$$

which is the same ~~and has the same attributes~~ as Eq. (27), ~~only~~ but with the freezing indices ~~are used~~ instead of the thawing ones.

Appendix C

Table C1. List of sites used for model evaluation.

Site	Region	Latitude [°]	Longitude [°]	Altitude [m asl]	Surface cover	Permafrost zone	Validation period	Years	MAPT [°C]	ALT [cm]	Source
Aiguille du Midi – NE	European Alps	45.87856	6.88833	3745	Bedrock	Mountain	2011–2015	5	−3.56	299.2	GTN-P
Aiguille du Midi – NW	European Alps	45.87864	6.88692	3738	Bedrock	Mountain	2010–2015	6	−4.83	206.7	GTN-P
Hoher Sonnblick 1	European Alps	47.05403	12.95752	3105	Bedrock	Mountain	2008–2011	4	−1.21	122.8	GTN-P
Hoher Sonnblick 3	European Alps	47.05351	12.95760	3079	Bedrock	Mountain	2016–2018	3	−1.95	110.7	GTN-P
Abernethy Flats	James Ross Island	−63.88138	-57.94832	41	Bare	Continuous	2014–2019	6	−6.36	62.5	MU
Berry Hill slopes	James Ross Island	−63.80267	-57.83863	56	Bare	Continuous	2018–2020	3	−5.24	84.2	MU
CALM	James Ross Island	−63.80190	-57.88460	10	Bare	Continuous	2015–2023	7	−4.74	87.1	MU
Johann Gregor Mendel	James Ross Island	−63.80152	-57.88330	10	Bare	Continuous	2012–2023	12	−5.13	61.3	MU
Johnson Mesa	James Ross Island	−63.82250	-57.93280	340	Bare	Continuous	2013–2023	11	−6.32	60.0	MU
Bull Pass	McMurdo Sound	−77.51847	161.86269	141	Bare	Continuous	2000–2022	22	−19.20	47.9	USDA
Granite Harbour	McMurdo Sound	−77.00655	162.52561	6	Bare	Continuous	2008–2015	4	−14.33	85.7	USDA
Marble Point	McMurdo Sound	−77.41955	163.68247	47	Bare	Continuous	2000–2022	20	−17.71	49.6	USDA
Endalen	Svalbard	78.19021	15.78158	40	Bare	Continuous	2009–2015	5	−2.25	142.1	GTN-P
Kapp Linne 2	Svalbard	78.05461	13.63667	21	Bare	Continuous	2009–2017	7	−2.15	186.5	GTN-P
Mould Bay 1	Prince Patrick Island	76.22869	−119.29893	36	Bare	Continuous	2008–2011	4	−13.53	59.7	GTN-P
Mould Bay 2	Prince Patrick Island	76.22869	−119.29893	36	Bare	Continuous	2008–2012	5	−13.47	58.4	GTN-P
Villum 1	Greenland	81.57928	−16.64330	36	Bare	Continuous	2015–2020	6	−7.03	96.1	GTN-P
Villum 2	Greenland	81.57958	−16.64752	27	Bare	Continuous	2015–2020	5	−6.30	110.2	GTN-P
Atqasuk	Alaska	70.45242	−157.41178	22	Grass	Continuous	2001–2010	9	−5.74	55.7	USDA
Barrow (site 1)	Alaska	71.32242	−156.61089	9	Grass	Continuous	1997–2017	16	−7.28	56.6	USDA
Betty Pingo: polygon center	Alaska	70.28258	−148.89347	12	Grass	Continuous	2006–2022	9	−6.12	42.3	USDA
Betty Pingo: polygon rim	Alaska	70.28258	−148.89347	12	Grass	Continuous	2006–2012	7	−5.98	52.1	USDA
Westdock (high): polygon center	Alaska	70.37039	−148.56867	3	Grass	Continuous	2004–2020	17	−6.56	58.5	USDA
Westdock (high): polygon rim	Alaska	70.37039	−148.56867	3	Grass	Continuous	2004–2020	17	−6.85	60.2	USDA
Westdock (high): polygon trough	Alaska	70.37039	−148.56867	3	Grass	Continuous	2004–2020	14	−6.42	49.9	USDA
Westdock (low): polygon trough	Alaska	70.37047	−148.56561	2	Grass	Continuous	2008–2022	9	−6.17	43.0	USDA
Old Auroral Station	Alaska	78.20146	15.83465	8	Grass	Continuous	2009–2015	7	−3.81	94.8	GTN-P
Petuniabukta	Svalbard	78.70306	16.46778	15	Grass	Continuous	2012–2018	7	−3.09	107.5	MU
QT01	Qinghai-Tibetan Plateau	35.14000	93.04000	4710	Grass	Discontinuous	2004–2013	10	−1.97	170.2	NTP/TPEDC
QT05	Qinghai-Tibetan Plateau	33.96000	92.34000	4620	Grass	Discontinuous	2004–2013	10	−0.20	310.7	NTP/TPEDC
QT09	Qinghai-Tibetan Plateau	35.72000	94.13000	4450	Grass	Discontinuous	2011–2018	8	−1.21	143.6	NTP/TPEDC
TSHAL	Qinghai-Tibetan Plateau	35.36000	79.55000	4850	Grass	Discontinuous	2016–2018	3	−2.87	149.8	NTP/TPEDC
Ivotuk 3	Alaska	68.47890	−155.73809	565	Shrub	Continuous	2011–2012	2	−2.33	57.8	GTN-P
Ivotuk 3–2	Alaska	68.47890	−155.73809	565	Shrub	Continuous	2011–2012	2	−1.84	55.4	GTN-P
Kugurak Cabin	Alaska	66.56238	−159.00464	7	Shrub	Continuous	2013–2013	1	−3.70	56.9	GI-UAF
Kuparuk Basin 03	Alaska	68.63490	−149.36393	820	Shrub	Continuous	2016–2017	2	−2.00	62.9	GI-UAF
Kuparuk Basin 1391	Alaska	68.64262	−149.38097	782	Shrub	Continuous	2016–2017	2	−1.41	85.6	GI-UAF
Kuparuk Basin 31	Alaska	68.63294	−149.36136	822	Shrub	Continuous	2016–2017	2	−1.42	67.1	GI-UAF
Bonanza Creek 1	Alaska	64.70694	−148.29128	125	Forest	Discontinuous	2012–2016	5	−0.73	65.9	GI-UAF
Fox	Alaska	64.95061	−147.61769	240	Forest	Discontinuous	2013–2015	3	−0.33	52.7	GI-UAF
Gakona 1	Alaska	62.39292	−145.14528	550	Forest	Continuous	2010–2014	5	−0.71	65.2	GI-UAF
Gakona 2	Alaska	62.39128	−145.14689	548	Forest	Continuous	2013–2013	1	−0.80	70.4	GI-UAF
Smith Lake	Alaska	64.86752	−147.85883	158	Forest	Discontinuous	2007–2011	5	−0.11	191.9	GTN-P

GTN-P = Global Terrestrial Network for Permafrost, MU = Polar-Geo-Lab of the Masaryk University, USDA = Natural Resources Conservation Service of the United States Department of Agriculture, NTP/TPEDC = National Tibetan Plateau/Third Pole Environment Data Center, GI-UAF = Geophysical Institute Permafrost Laboratory of the University of Alaska Fairbanks.

Data availability. The validation data from James Ross Island and Petuniabukta are available upon request from Filip Hrbáček (hrbacek-filip@gmail.com) and Kamil Láska (laska@sci.muni.cz), respectively, while the other data are available from Global Terrestrial Network for Permafrost (http://gtnpdatabase.org), Natural Resources Conservation Service of the United States Department of Agriculture (https://www.nrcs.usda.gov/resources/data-and-reports/soil-climate-research-stations), Geophysical Institute Permafrost Laboratory of the University of Alaska Fairbanks (https://permafrost.gi.alaska.edu), and National Tibetan Plateau/Third Pole Environment Data Center (https://data.tpdc.ac.cn/en/disallow/789e838e-16ac-4539-bb7e-906217305a1d).

Author contributions. TU: conceptualization, methodology, software, validation, formal analysis, resources, investigation, writing – original draft, visualization. FH: conceptualization, resources, writing – review & editing, supervision, funding acquisition. MK: formal analysis, resources, writing – review & editing.

Competing interests. The contact author has declared that none of the authors has any competing interests.

Acknowledgements. We ~~acknowledge USDA for access to the soil climate data from the McMurdo Sound and North Slope of Alaska~~ thank Kamil Láska and acknowledge the Global Terrestrial Network for Permafrost, Natural Resources Conservation Service of the United States Department of Agriculture, Geophysical Institute Permafrost Laboratory of the University of Alaska Fairbanks and National Tibetan Plateau/Third Pole Environment Data Center for collecting long-term ground temperature data and disseminating them personally and/or publicly.

Financial support. The research was funded by the Czech Science Foundation (project number GM22-28659M).

References

Aalto, J., Karjalainen, O., Hjort, J., and Luoto, M.: Statistical forecasting of current and future Circum-Arctic ground temperatures and active layer thickness, Geophys. Res. Lett., 45, 4889–4898, 2018.

Anisimov, O. A., Shiklomanov, N. I., and Nelson, F. E.: Global warming and active-layer thickness: results from transient general circulation models, Glob. Planet. Change, 15, 61–77, https://doi.org/10.1016/S0921-8181(97)00009-X, 1997.

Anisimov, O. A., Shiklomanov, N. I., and Nelson, F. E.: Variability of seasonal thaw depth in permafrost regions: a stochastic modeling approach, Ecol. Model., 153, 217–227, https://doi.org/10.1016/S0304-3800(02)00016-9, 2002.

Biskaborn, B. K., Lanckman, J.-P., Lantuit, H., Elger, K., Streletskiy, D. A., Cable, W. L., and Romanovsky, V. E.: The new database of the Global Terrestrial Network for Permafrost (GTN-P), Earth Syst. Sci. Data, 7, 245–259, https://doi.org/10.5194/essd-7-245-2015, 2015.

Biskaborn, B. K., Smith, S. L., Noetzli, J., Matthes, H., Vieira, G., Streletskiy, D. A., Schoeneich, P., Romanovsky, V. E., Lewkowicz, A. G., Abramov, A., Allard, M., Boike, J., Cable, W. L., Christiansen, H. H., Delaloye, R., Diekmann, B., Drozdov, D., Etzelmüller, B., Grosse, G., Guglielmin, M., Ingeman-Nielsen, T., Isaksen, K., Ishikawa, M., Johansson, M., Johansson, H., Joo, A., Kaverin, D., Kholodov, A., Konstantinov, P., Kröger, T., Lambiel, C., Lanckman, J.-P., Luo, D., Malkova, G., Meiklejohn, I., Moskalenko, N., Oliva, M., Phillips, M., Ramos, M., Sannel, A. B. K., Sergeev, D., Seybold, C., Skryabin, P., Vasiliev, A., Wu, Q., Yoshikawa, K., Zheleznyak, M., and Lantuit, H.: Permafrost is warming at a global scale, Nat. Commun., 10, 264, https://doi.org/10.1038/s41467-018-08240-4, 2019.

Bonnaventure, P. P. and Lamoureux, S. F.: The active layer: A conceptual review of monitoring, modelling techniques and changes in a warming climate, Prog. Phys. Geog., 37, 352–376, https://doi.org/10.1177/0309133313478314, 2013.

Brown, J., Hinkel, K. M., and Nelson, F. E.: The circumpolar active layer monitoring (calm) program: Research designs and initial results, Polar Geogr., 24, 166–258, https://doi.org/10.1080/10889370009377698, 2000.

Burn, C. R.: The Active Layer: Two Contrasting Definitions, Permafrost Periglac., 9, 411–416, https://doi.org/10.1002/(SICI)1099-1530(199810/12)9:4<411::AID-PPP292>3.0.CO;2-6, 1998.

Burn, C.R.and Smith, C.A. S.: Observations of the "Thermal Offset" in Near-Surface Mean Annual Ground Temperatures at Several Sites near Mayo, Yukon Territory, Canada, Arctic, 41, 99–104,

Cao, B., Gruber, S., Zheng, D., and Li, X.: The ERA5-Land soil temperature bias in permafrost regions, The Cryosphere, 14, 2581–2595, https://www.jstor.doi.org/stable10.5194/40510685, 1988. tc-14-2581-2020, 2020.

Carslaw, H. S. and Jaeger, J. C.: Conduction of Heat in Solids, Second Edition, Oxford University Press, Oxford, United Kingdom, 520 pp., 1959.

de Pablo, M. A., Ramos, M., Molina, A., and Prieto, M.: Thaw depth spatial and temporal variability at the Limnopolar Lake CALM-S site, Byers Peninsula, Livingston Island, Antarctica, Sci. Total Environ., 615, 814–827, https://doi.org/10.1016/j.scitotenv.2017.09.284, 2018.

Farzamian, M., Vieira, G., Monteiro Santos, F. A., Yaghoobi Tabar, B., Hauck, C., Paz, M. C., Bernardo, I., Ramos, M., and de Pablo, M. A.: Detailed detection of active layer freeze–thaw dynamics using quasi-continuous electrical resistivity tomography (Deception Island, Antarctica), The Cryosphere, 14, 1105–1120, https://doi.org/10.5194/tc-14-1105-2020, 2020.

Ferreira, A., Vieira, G., Ramos, M., and Nieuwendam, A.: Ground temperature and permafrost distribution in Hurd Peninsula (Livingston Island, Maritime Antarctic): An assessment using freezing indexes and TTOP modelling, Catena, 149, 560–571, http://dx.doi.org/10.1016/j.catena.2016.08.027, 2017.

Gao, Z., Lin, Z., Niu, F., and Luo, J.: Soil water dynamics in the active layers under different land-cover types in the permafrost regions of the Qinghai–Tibet Plateau, China. Geoderma, 364, 114176, https://doi.org/10.1016/j.geoderma.2020.114176, 2020.

Garagulya, L. S.: Application of Mathematical Methods and Computers in Investigations of Geocryological Processes, Moscow University Press, Moscow, Russia, 124 pp., 1990.

Garibaldi, M. C., Bonnaventure, P. P., and Lamoureux, S. F.: Utilizing the TTOP model to understand spatial permafrost temperature variability in a High Arctic landscape, Cape Bounty, Nunavut, Canada, Permafrost Periglac., 32, 19–34, https://doi.org/10.1002/ppp.2086, 2021.

Gisnås, K., Etzelmüller, B., Farbrot, H., Schuler, T. V., and Westermann, S.: CryoGRID 1.0: Permafrost Distribution in Norway estimated by a Spatial Numerical Model, Permafrost Periglac., 24, 2–19, https://doi.org/10.1002/ppp.1765, 2013.

~~Goodrich, L. E.: The influence of snow cover on the ground thermal regime, Can. Geotech. J., 19, 421–432, https://doi.org/10.1139/t82-047, 1982.~~

Grosse, G., Goetz, S., McGuire, A. D., Romanovsky, V. E., and Schuur, E. A. G.: Changing permafrost in a warming world and feedbacks to the Earth system, Environ. Res. Lett., 11, 040201, https://doi.org/10.1088/1748-9326/11/4/040201, 2016.

Hauck, C.: Frozen ground monitoring using DC resistivity tomography, Geophys. Res. Lett., 29, 2016, https://doi.org/10.1029/2002GL014995, 2002.

Hayashi, M., Goeller, N., Quinton, W. L., and Wright, N.: A simple heat-conduction method for simulating the frost-table depth in hydrological models, Hydrol. Process., 21, 2610–2622, https://doi.org/10.1002/hyp.6792, 2007.

Hinkel, K. M., Nicholas, J. R. J.: Active Layer Thaw Rate at a Boreal Forest Site in Central Alaska, U.S.A., Arct. Alp. Res., 27, 72–80, https://doi.org/10.2307/1552069, 1995.

Hjort, J., Streletskiy, D., Doré, G., Wu, Q., Bjella, K., and Luoto, M.: Impacts of permafrost degradation on infrastructure, Nat. Rev. Earth Environ., 3, 24–38, https://doi.org/10.1038/s43017-021-00247-8, 2022.

Hrbáček, F. and Uxa, T.: The evolution of a near-surface ground thermal regime and modeled active-layer thickness on James Ross Island, Eastern Antarctic Peninsula, in 2006–2016, Permafrost Periglac., 31, 141–155, https://doi.org/10.1002/ppp.2018, 2020.

Hrbáček, F., Kňažková, M., Nývlt, D., Láska, K., Mueller, C. W., and Ondruch, J.: Active layer monitoring at CALM-S site near J. G. Mendel Station, James Ross Island, eastern Antarctic Peninsula, Sci. Total Environ., 601–602, 987–997, https://doi.org/10.1016/j.scitotenv.2017.05.266, 2017a.

Hrbáček, F., Nývlt, D., and Láska, K.: Active layer thermal dynamics at two lithologically different sites on James Ross Island, Eastern Antarctic Peninsula, Catena, 149, 592–602, https://doi.org/10.1016/j.catena.2016.06.020, 2017b.

Hrbáček, F., Cannone, N., Kňažková, M., Malfasi, F., Convey, P., and Guglielmin, M.: Effect of climate and moss vegetation on ground surface temperature and the active layer among different biogeographical regions in Antarctica, Catena, 190, 104562, https://doi.org/10.1016/j.catena.2020.104562, 2020.

Hrbáček, F., Engel, Z., Kňažková, M., and Smolíková, J.: Effect of summer snow cover on the active layer thermal regime and thickness on CALM-S JGM site, James Ross Island, eastern Antarctic Peninsula, Catena, 207, 105608, https://doi.org/10.1016/j.catena.2021.105608, 2021.

Hrbáček, F., Kňažková, M., Farzamian, M., and Baptista, J.: Variability of soil moisture on three sites in the Northern Antarctic Peninsula in 2022/23, Czech Polar Rep., 13, 10–23, https://doi.org/10.5817/CPR2023-1-2, 2023a.

Hrbáček, F., Oliva, M., Hansen, C., Balks, M., O'Neill, T. A., de Pablo, M. A., Ponti, S., Ramos, M., Vieira, G., Abramov, A., Kaplan Pastíriková, L., Guglielmin, M., Goyanes, G., Rocha Francelino, M., Schaefer, C., and Lacelle, D.: Active layer and permafrost thermal regimes in the ice-free areas of Antarctica, Earth-Sci. Rev., 242, 104458, https://doi.org/10.1016/j.earscirev.2023.104458, 2023b.

Hrbáček, F., Kňažková, M., Láska, K., and Kaplan Pastíriková, L.: Active Layer Warming and Thickening on CALM-S JGM, James Ross Island, in the Period 2013/14–2022/23, Permafrost Periglac., https://doi.org/10.1002/ppp.2274, 2025.

Horton, R., Wierenga, P. J., and Nielsen, D. R.: Evaluation of Methods for Determining the Apparent Thermal Diffusivity of Soil Near the Surface, Soil. Sci. Soc. Am. J., 47, 25–32, https://doi.org/10.2136/sssaj1983.03615995004700010005x, 1983.

Kaplan Pastíriková, L., Hrbáček, F., Uxa, T., and Láska, K.: Permafrost table temperature and active layer thickness variability on James Ross Island, Antarctic Peninsula, in 2004–2021, Sci. Total Environ., 869, 161690, https://doi.org/10.1016/j.scitotenv.2023.161690, 2023.

Kaplan Pastíriková, L., Hrbáček, F., and Matějka, M.: Validation of ERA5-Land-based reconstructed air temperature and near-surface ground temperature on James Ross Island. Polar Geogr., 1–21, https://doi.org/10.1080/1088937X.2024.2434744, 2024.

Kňažková, M. and Hrbáček, F.: Interannual variability of soil thermal conductivity and moisture on the Abernethy Flats (James Ross Island) during thawing seasons 2015–2023, Catena, 234, 107640, https://doi.org/10.1016/j.catena.2023.107640, 2024.

Kudryavtsev, V. A., Garagulia, L., Kondratyeva, K. A., and Melamed, V. G.: Fundamentals of Frost Forecasting in Geological Engineering Investigations, Draft Translation 606, U.S. Army Cold Regions Research And Engineering Lab, Hanover, NH, 489 pp., 1977.

Kurylyk, B. L.: Discussion of 'A Simple Thaw-Freeze Algorithm for a Multi-Layered Soil using the Stefan Equation' by Xie and Gough (2013), Permafrost Periglac., 26, 200–206, https://doi.org/10.1002/ppp.1834, 2015.

Lacelle, D., Lapalme, C., Davila, A. F., Pollard, W., Marinova, M., Heldmann, J., and McKay, C. P.: Solar radiation and air and ground temperature relations in the cold and hyper-arid Quartermain Mountains, McMurdo Dry Valleys of Antarctica, Permafrost Periglac., 27, 163–176, https://doi.org/10.1002/ppp.1859, 2016.

Lawrence, D. M., Koven, C. D., Swenson, S. C., Riley, W. J., and Slater, A. G.: Permafrost thaw and resulting soil moisture changes regulate projected high-latitude CO_2 and CH_4 emissions, Environ. Res. Lett., 10, 094011, https://doi.org/10.1088/1748-9326/10/9/094011, 2015.

Li, G., Zhang, M., Pei, W., Melnikov, A., Khristoforov, I., Li, R., and Yu, F.: Changes in permafrost extent and active layer thickness in the Northern Hemisphere from 1969 to 2018, Sci. Total Environ., 804, 150182, https://doi.org/10.1016/j.scitotenv.2021.150182, 2022.

Li, W., Weng, B., Yan, D., Lai, Y., Li, M., and Wang, H.: Underestimated permafrost degradation: Improving the TTOP model based on soil thermal conductivity, Sci. Total Environ., 854, 158564, https://doi.org/10.1016/j.scitotenv.2022.158564, 2023.

Lunardini, V.J.: Theory of N-factors and correlation of data, in: Proceedings of the 3rd International Conference on Permafrost, Edmonton, Canada, 10–13 July 1978, 40–46, 1978.

Liu, Z., Guo, D., Hua, W., and Chen, Y.: Near-surface permafrost extent and active layer thickness characterized by reanalysis/assimilation data. Atmos. Sci. Lett., 26, e1289. https://doi.org/10.1002/asl.1289, 2025.

Lunardini, V. J.: Heat Transfer in Cold Climates, Van Nostrand Reinhold Co., New York, NY, 731 pp., 1981.

Nelson, F. E. and Outcalt, S. I.: A Computational Method for Prediction and Regionalization of Permafrost, Arctic Alpine Res., 19, 279–288, https://doi.org/10.2307/1551363, 1987.

Nelson, F. E., Shiklomanov, N. I., Mueller, G., Hinkel, K. M., Walker, D. A., and Bockheim, J. G.: Estimating Active-Layer Thickness over a Large Region: Kuparuk River Basin, Alaska, U.S.A., Arct. Alp. Res., 29, 367–378, https://doi.org/10.2307/1551985, 1997.

Neumann, F.: Lectures given in the 1860's, cf. Riemann-Weber, Die Partiellen Differentialgleichungen der Mathematischen, Physik, 2, 117–121.–

Nicolsky, D.J., Romanovsky, V. E., and Panteleev, G. G.: Estimation of soil thermal properties using in-situ temperature measurements in the active layer and permafrost, Cold Reg. Sci. Technol., 55, 120–129, https://doi.org/10.1016/j.coldregions.2008.03.003, 2009. c. 1860.

Noetzli, J., Arenson, L. U., Bast, A., Beutel, J., Delaloye, R., Farinotti, D., Gruber, S., Gubler, H., Haeberli, W., Hasler, A., Hauck, C., Hiller, M., Hoelzle, M., Lambiel, C., Pellet, C., Springman, S. M., Vonder Muehll, D., and Phillips, M.: Best Practice for Measuring Permafrost Temperature in Boreholes Based on the Experience in the Swiss Alps, Front. Earth Sci., 9, 607875, https://doi.org/10.3389/feart.2021.607875, 2021.

Noetzli, J., Christiansen, H. H., Guglielmin, M., Hrbáček, F., Hu, G., Isaksen, K., Magnin, F., Pogliotti, P., Smith, S. L., Zhao, L., and Streletskiy, D. A.: Permafrost temperature and active-layer thickness, in: State of the Climate in 2023, Bull. Amer. Meteor. Soc., 105, S43–S44. https://doi.org/10.1175/2024BAMSStateoftheClimate.1, 2024.

Obu, J.: How Much of the Earth's Surface is Underlain by Permafrost?, J. Geophys. Res.–Earth, 126, e2021JF006123, https://doi.org/10.1029/2021JF006123, 2021.

Obu, J., Westermann, S., Bartsch, A., Berdnikov, N., Christiansen, H. H., Dashtseren, A., Delaloye, R., Elberling, B., Etzelmüller, B., Kholodov, A., Khomutov, A., Kääb, A., Leibman, M. O., Lewkowicz, A. G., Panda, S. K., Romanovsky, V., Way, R. G., Westergaard-Nielsen, A., Wu, T., Yamkhin, J., and Zou, D.: Northern Hemisphere permafrost map based on TTOP modelling for 2000–2016 at 1 km^2 scale, Earth Sci. Rev., 193, 299–316, https://doi.org/10.1016/j.earscirev.2019.04.023, 2019.

Obu, J., Westermann, S., Vieira, G., Abramov, A., Balks, M. R., Bartsch, A., Hrbáček, F., Kääb, A., and Ramos, M.: Pan-Antarctic map of near-surface permafrost temperatures at 1 km^2 scale, The Cryosphere, 14, 497–519, https://doi.org/10.5194/tc-14-497-2020, 2020.

Peng, X., Zhang, T., Frauenfeld, O. W., Mu, C., Wang, K., Wu, X., Guo, D., Luo, J., Hjort, J., Aalto, J., Karjalainen, O., and Luoto, M.: Active Layer Thickness and Permafrost Area Projections for the 21st Century, Earth's Future, 11, e2023EF003573, https://doi.org/10.1029/2023EF003573, 2023.

Riseborough, D.: Thawing and freezing indices in the active layer, in: Proceedings of the 8th International Conference on Permafrost, Zurich, Switzerland, 21–25 July 2003, ~~953-–958~~953–958, 2003.

Riseborough, D. W.: Exploring the parameters of a simple model of the permafrost-climate relationship, Ph.D. thesis, Carleton University, Ottawa, 328 pp., 2004.

Riseborough, D.: The effect of transient conditions on an equilibrium permafrost-climate model. Permafrost Periglac., 18, 21–32, https://doi.org/10.1002/ppp.579, 2007.

Riseborough, D. W.: Estimating active layer and talik thickness from temperature data: implications from modeling results, in: Proceedings of the 9th International Conference on Permafrost, Fairbanks, Alaska, 29 June–3 July 2008, 1487–1492, 2008.

Riseborough, D., Shiklomanov, N., Etzelmüller, B., Gruber, S., and Marchenko, S.: Recent advances in permafrost modelling, Permafrost Periglac., 19, 137–156, https://doi.org/10.1002/ppp.615, 2008.

Romanovsky, V. E. and Osterkamp, T. E.: Interannual Variations of the Thermal Regime of the Active Layer and Near-Surface Permafrost in Northern Alaska, Permafrost Periglac., 6, 313–335, https://doi.org/10.1002/ppp.3430060404, 1995.

Romanovsky, V. E. and Osterkamp, T. E.: Thawing of the Active Layer on the Coastal Plain of the Alaskan Arctic, Permafrost Periglac., 8, 1–22, https://doi.org/10.1002/(SICI)1099-1530(199701)8:1<1::AID-PPP243>3.0.CO;2-U, 1997.

Sazonova, T. S. and Romanovsky, V. E.: A model for regional-scale estimation of temporal and spatial variability of active layer thickness and mean annual ground temperaturesPermafrost Periglac., 14, 125–139, https://doi.org/10.1002/ppp.449, 2003.

Schuur, E. A., Abbott, B. W., Commane, R., Ernakovich, J., Euskirchen, E., Hugelius, G., Grosse, G., Jones, M., Koven, C., Leshyk, V., Lawrence, D., Loranty, M. M., Mauritz, M., Olefeldt, D., Natali, S., Rodenhizer, H., Salmon, V., Schädel, C., Strauss, J., Treat, C., and

Turetsky, M.: Permafrost and Climate Change: Carbon Cycle Feedbacks From the Warming Arctic, Annu. Rev. Env. Resour., 47, 343–371, https://doi.org/10.1146/annurev-environ-012220-011847, 2022.

Shiklomanov, N. I. and Nelson, F. E.: Active-Layer Mapping at Regional Scales: A 13-Year Spatial Time Series for the Kuparuk Region, North-Central Alaska, Permafrost Periglac., 13, 219–230, https://doi.org/10.1002/ppp.425, 2002.

Shiklomanov, N. I., Streletskiy, D. A., Nelson, F. E., Hollister, R. D., Romanovsky, V. E., Tweedie, C. E., Bockheim, J. G., and Brown, J.: Decadal variations of active-layer thickness in moisture-controlled landscapes, Barrow, Alaska, J. Geophys. Res.-Biogeo., 115, G00I04, https://doi.org/10.1029/2009JG001248, 2010.

Smith, M. W. and Riseborough, D. W.: Permafrost monitoring and detection of climate change, Permafrost Periglac., 7, 301–309, https://doi.org/10.1002/(SICI)1099-1530(199610)7:4<301::AID-PPP231>3.0.CO;2-R, 1996.

Smith, S. L., Wolfe, S. A., Riseborough, D. W., and Nixon, F. M.: Active-layer characteristics and summer climatic indices, Mackenzie Valley, Northwest Territories, Canada. Permafrost Periglac., 20, 201–220, https://doi.org/10.1002/ppp.651, 2009.

Smith, S. L., O'Neill, H. B., Isaksen, K., Noetzli, J., and Romanovsky, V. E.: The changing thermal state of permafrost, Nat. Rev. Earth Environ., 3, 10–23, https://doi.org/10.1038/s43017-021-00240-1, 2022.

Smith, S. L., Romanovsky, V. E., Isaksen, K., Nyland, K., Shiklomanov, N. I., Streletskiy, D. A., and Christiansen, H. H.: Permafrost (Arctic), in: State of the Climate in 2023, Bull. Amer. Meteor. Soc., 105, S314–S317. https://doi.org/10.1175/BAMS-D-24-0101.1, 2024

Stefan, J.: Über die Theorie der Eisbildung, insbesondere über die Eisbildung im Polarmeere, Ann. Phys., 278, 269–286, https://doi.org/10.1002/andp.18912780206, 1891.

Streletskiy, D. A., Shiklomanov, N. I., and Nelson, F. E.: Spatial variability of permafrost active-layer thickness under contemporary and projected climate in northern Alaska, Polar Geogr., 35, 95–116, https://doi.org/10.1080/1088937X.2012.680204, 2012.

Sun, Z., Zhao,

Streletskiy, D., Noetzli, J., Smith, S. L., Hu, G. , Qiao, Y., Du, E., Zou, DVieira, G., Schoeneich, P., Hrbacek, F., and Xie, C. : Modeling permafrost changes on the Qinghai-Tibetan plateau from 1966 to 2100: A case study from two boreholes along the Qinghai-Tibet engineering corridor, Permafrost Periglac., 31, 156–171, Irrgang, A. M.: Measurement Recommendations and Guidelines for the Global Terrestrial Network for Permafrost (GTN-P), Zenodo, https://doi.org/10.100210.5281/ppp.2022, 2020. zenodo.5973079, 2022.

Walvoord, M. A., Kurylyk, B.L.: Hydrologic Impacts of Thawing Permafrost—A Review, Vadose Zone J., 15, vzj2016-01, https://doi.org/10.2136/vzj2016.01.0010, 2016.

Wang, C., Wang, Z., Kong, Y., Zhang, F., Yang, K., and Zhang, T.: Most of the Northern Hemisphere Permafrost Remains under Climate Change, Sci. Rep., 9, 3295, https://doi.org/10.1038/s41598-019-39942-4, 2019.

Wang, K., Jafarov, E., and Overeem, I.: Sensitivity evaluation of the Kudryavtsev permafrost model, Sci. Total Environ., 720, 137538, https://doi.org/10.1016/j.scitotenv.2020.137538, 2020.

Way, R. G. and Lewkowicz, A. G.: Environmental controls on ground temperature and permafrost in Labrador, northeast Canada, Permafrost Periglac., 29, 73–85, https://doi.org/10.1002/ppp.1972, 2018.

Wenhao, L., Ren, L., Tonghua, W., Xiaoqian, S., Xiaodong, W., Guojie, H., Lin, Z., Jimin, Y., Dong, W., Yao, X., Jianzong, S., Junjie, M., Shenning, W., and Yongping, Q.: Spatio-temporal variation in soil thermal conductivity during the freeze-thaw period in the permafrost of the Qinghai–Tibet Plateau in 1980–2020, Sci. Total Environ., 913, 169654, https://doi.org/10.1016/j.scitotenv.2023.169654, 2024.

Yin, G., Niu, F., Lin, Z., Luo, J., and Liu, M.: Performance comparison of permafrost models in Wudaoliang Basin, Qinghai-Tibet plateau, China, J. Mt. Sci., 13, 1162–1173, https://doi.org/10.1007/s11629-015-3745-x, 2016.

Zhao, S. P., Nan, Z. T., Huang, Y. B., and Zhao, L.: The Application and Evaluation of Simple Permafrost Distribution Models on the Qinghai–Tibet Plateau, Permafrost Periglac., 28, 391–404, https://doi.org/10.1002/ppp.1939, 2017.

Zhao, L., Zou, D., Hu, G., Wu, T., Du, E., Liu, G., Xiao, Y., Li, R., Pang, Q., Qiao, Y., Wu, X., Sun, Z., Xing, Z., Sheng, Y., Zhao, Y., Shi, J., Xie, C., Wang, L., Wang, C., and Cheng, G.: A synthesis dataset of permafrost thermal state for the Qinghai–Tibet (Xizang) Plateau, China, Earth Syst. Sci. Data, 13, 4207–4218, https://doi.org/10.5194/essd-13-4207-2021, 2021.

Zorigt, M., Kwadijk, J., Van Beek, E., and Kenner, S.: Estimating thawing depths and mean annual ground temperatures in the Khuvsgul region of Mongolia, Environ. Earth Sci., 75, 897, https://doi.org/10.1007/s12665-016-5687-1, 2016.